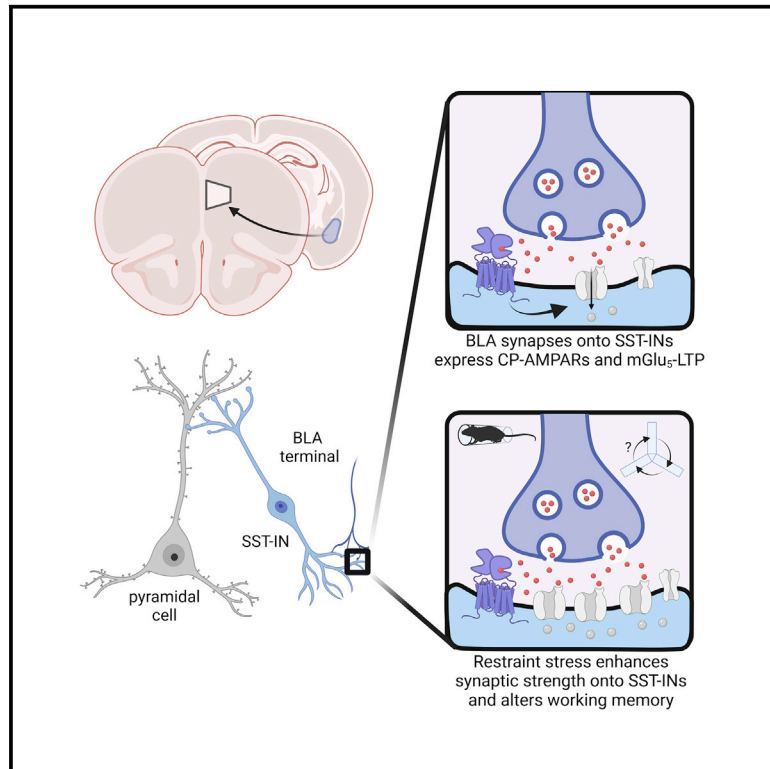


Acute restraint stress redirects prefrontal cortex circuit function through mGlu₅ receptor plasticity on somatostatin-expressing interneurons

Graphical abstract



Authors

Max E. Joffe, James Maksymetz, Joseph R. Lusching, ..., Michael R. Tadross, Danny G. Winder, P. Jeffrey Conn

Correspondence

joffeme@upmc.edu (M.E.J.),
jeff.conn@vanderbilt.edu (P.J.C.)

In brief

Joffe et al. demonstrated that restraint stress rapidly potentiates excitatory transmission onto prefrontal cortex somatostatin interneurons in mice, biasing information processing toward amygdala-driven feedforward inhibition. The authors pinpoint metabotropic glutamate mGlu₅ receptor plasticity on somatostatin interneurons as an essential mediator of microcircuit modifications and discrete behavioral adaptations following acute stress.

Highlights

- Restraint stress activates PFC SST-INS
- Restraint stress enhances excitatory drive onto SST-INS and feedforward inhibition
- mGlu₅ receptors regulate LTP on SST-INS
- SST-mGlu₅^{-/-} mice display unique stress-related behavioral adaptations

Article

Acute restraint stress redirects prefrontal cortex circuit function through mGlu₅ receptor plasticity on somatostatin-expressing interneurons

Max E. Joffe,^{1,2,15,16,*} James Maksymetz,^{3,4,5} Joseph R. Lusching,^{6,7} Shalini Dogra,^{3,4} Anthony S. Ferranti,^{3,4} Deborah J. Luessen,^{3,4} Isabel M. Gallinger,^{3,4} Zixiu Xiang,^{3,4} Hannah Branthwaite,³ Patrick R. Melugin,³ Kellie M. Williford,^{3,6} Samuel W. Centanni,^{6,7} Brenda C. Shields,^{8,9} Craig W. Lindsley,^{3,4,6,10,11} Erin S. Calipari,^{3,6,7,12,13} Cody A. Siciliano,^{3,6,13} Colleen M. Niswender,^{3,4,12,13,14} Michael R. Tadross,^{8,9} Danny G. Winder,^{3,6,7,13} and P. Jeffrey Conn^{3,4,6,13,14,*}

¹Department of Psychiatry, University of Pittsburgh, Pittsburgh, PA 15219, USA

²Translational Neuroscience Program, University of Pittsburgh, Pittsburgh, PA, USA

³Department of Pharmacology, Vanderbilt University, Nashville, TN 37232, USA

⁴Warren Center for Neuroscience Drug Discovery, Nashville, TN, USA

⁵Department of Neuroscience, Genentech, Inc., South San Francisco, CA 94080, USA

⁶Vanderbilt Center for Addiction Research, Nashville, TN, USA

⁷Department of Molecular Physiology and Biophysics, Vanderbilt University, Nashville, TN, USA

⁸Department of Neurobiology, Duke University, Durham, NC 27708, USA

⁹Department of Biomedical Engineering, Duke University, Durham, NC, USA

¹⁰Department of Chemistry, Vanderbilt University, Nashville, TN, USA

¹¹Vanderbilt Institute of Chemical Biology, Vanderbilt University, Nashville, TN, USA

¹²Department of Psychiatry, Vanderbilt University Medical Center, Nashville, TN, USA

¹³Vanderbilt Brain Institute, Vanderbilt University, Nashville, TN, USA

¹⁴Vanderbilt Kennedy Center, Vanderbilt University Medical Center, Nashville, TN, USA

¹⁵Twitter: @mejoffe

¹⁶Lead contact

*Correspondence: joffeme@upmc.edu (M.E.J.), jeff.conn@vanderbilt.edu (P.J.C.)

<https://doi.org/10.1016/j.neuron.2021.12.027>

SUMMARY

Inhibitory interneurons orchestrate prefrontal cortex (PFC) activity, but we have a limited understanding of the molecular and experience-dependent mechanisms that regulate synaptic plasticity across PFC microcircuits. We discovered that mGlu₅ receptor activation facilitates long-term potentiation at synapses from the basolateral amygdala (BLA) onto somatostatin-expressing interneurons (SST-INs) in mice. This plasticity appeared to be recruited during acute restraint stress, which induced intracellular calcium mobilization within SST-INs and rapidly potentiated postsynaptic strength onto SST-INs. Restraint stress and mGlu₅ receptor activation each augmented BLA recruitment of SST-IN phasic feedforward inhibition, shunting information from other excitatory inputs, including the mediodorsal thalamus. Finally, studies using cell-type-specific mGlu₅ receptor knockout mice revealed that mGlu₅ receptor function in SST-expressing cells is necessary for restraint stress-induced changes to PFC physiology and related behaviors. These findings provide new insights into interneuron-specific synaptic plasticity mechanisms and suggest that SST-IN microcircuits may be promising targets for treating stress-induced psychiatric diseases.

INTRODUCTION

Stress can alter motivated behaviors through dynamic adaptations within the prefrontal cortex (PFC) (Liston et al., 2009; Sinha et al., 2016; Soares et al., 2012); however, much remains to be learned regarding the cellular and molecular mechanisms that mediate these alterations in circuit function. Most neurons within PFC are glutamatergic pyramidal cells that drive behaviors through their interactions with subcortical structures (Gabbott

et al., 2005; Sesack et al., 1989). In general, mechanistic studies have focused on the physiology, form, and function of pyramidal cells, revealing that stress can alter synaptic plasticity and dendritic spine stability (Duman et al., 2016; Holmes and Wellman, 2009; McEwen and Morrison, 2013). By contrast, although local inhibitory interneurons are vital for modulating pyramidal cell activity, how specific interneuron subtypes adapt during stressful experiences remains unclear. Furthermore, the breadth of literature implicating interneuron pathophysiology in the etiology of

many psychiatric diseases (Fogaça and Duman, 2019; Lewis et al., 2012; Luscher et al., 2011; Prévot and Sibille, 2021) provides compelling rationale for mechanistic research investigating how stressful experiences alter PFC inhibitory microcircuits.

A key population of neocortical GABAergic interneurons is defined by the restricted expression of the neuropeptide somatostatin interneurons (SST-INs) (Tremblay et al., 2016; Urban-Ciecko and Barth, 2016; Yavorska and Wehr, 2016). One of the major types of SST-IN is the Martinotti cell, which can be functionally characterized by low-threshold spiking activity as well as cellular anatomy, morphology, and function (Nigro et al., 2018). Martinotti cells provide feedback inhibition of excitatory transmission and plasticity through projections onto the apical dendrites of neighboring pyramidal cells (Higley, 2014; Marlin and Carter, 2014; Urban-Ciecko et al., 2015). Although SST-INs are driven by collaterals from local pyramidal cells, recent studies have indicated SST-INs also receive excitatory projections from subcortical areas. In particular, basolateral amygdala (BLA) afferents have emerged as being well suited to modulate SST-IN activity (McGarry and Carter, 2016) and have long been known to drive feedforward inhibition in PFC (Floresco and Tse, 2007; Ji et al., 2010; Pérez-Jaranay and Vives, 1991). These studies raise the possibility that SST-INs may guide heterosynaptic information processing within PFC and thus facilitate adaptive behaviors related to stress. Consistent with this possibility, PFC SST-INs have been implicated in various affective behaviors in rodent models (Ali et al., 2020; Cichon et al., 2017; Cummings and Clem, 2020; Fogaça et al., 2021; Scheggia et al., 2020; Soumier and Sibille, 2014; Xu et al., 2019). However, few studies have identified the cellular mechanisms that guide synaptic plasticity across these microcircuit elements and examined whether these circuits undergo specific adaptations in response to stress.

To address this gap, we utilized a combination of transgenic, optogenetic, and pharmacologic tools to interrogate PFC interneuron synaptic plasticity and circuit function. We found that the activation of mGlu₅ subtype metabotropic glutamate (mGlu) receptors facilitates long-term potentiation (LTP) of excitatory transmission onto PFC SST-INs. This synaptic adaptation occurs readily following acute restraint stress and biases information processing within PFC toward BLA-driven feedforward inhibition and away from excitatory drive from the mediodorsal thalamus (MDT). In turn, cognitive behavioral adaptations following acute restraint stress were absent in SST-mGlu₅^{-/-} mice. These findings highlight how discrete adaptations within microcircuit components can exert widespread effects on neural circuit function, provide new insights into interneuron-specific synaptic plasticity mechanisms, and may inform the development of novel treatments for psychiatric diseases.

RESULTS

mGlu₅ metabotropic glutamate receptors facilitate long-term potentiation (LTP) on PFC SST-INs

Studies in hippocampus have revealed that mGlu₁ and mGlu₅ receptors regulate LTP on SST-INs (Le Duigou and Kullmann, 2011; McBain et al., 1994; Pelkey et al., 2017; Perez et al.,

2001). To our knowledge, however, these signaling events have not been characterized in the PFC. We bred mice to express tdTomato fluorescent protein in SST-INs and recorded from labeled cells in deep layer prelimbic cortex (Joffe et al., 2020b; Figure 1A). Approximately 75% of SST-INs displayed low-threshold spiking phenotypes consistent with Martinotti cells (Figure 1B; Table S1). Fast-spiking-like or irregular cells were discarded. Consistent with research in hippocampus, application of the orthosteric mGlu_{1/5} agonist dihydroxyphenylglycine (DHPG) induced LTP of the evoked excitatory postsynaptic current (EPSC) (Figures 1C, 1D, and 1E). LTP persisted in the presence of the selective mGlu₁ negative allosteric modulator (NAM) VU0469650 but was blocked by the mGlu₅ NAM MTEP (Figure 1F), indicating critical and specific involvement of mGlu₅ receptors in regulating SST-IN LTP. In control recordings, LTP magnitude inversely correlated with the EPSC coefficient of variation (CV) (Figure 1G) but not with the paired-pulse ratio (PPR) (Figure 1H), suggesting a postsynaptic mechanism. Including the divalent ion chelator BAPTA in the patch pipette completely blocked LTP (Figures 1I and 1J), consistent with a critical function for postsynaptic calcium signaling in SST-IN LTP.

mGlu₅ receptor activation enhances amygdalo-cortical feedforward inhibition

We next probed what ramifications this synaptic plasticity would have for the integration of subcortical information within PFC. We addressed this question by expressing ChR2 via adeno-associated virus (AAV) delivery to the BLA or MDT (representative images can be found in Maksymetz et al. [2019]), followed by acute slice preparation and whole-cell recordings from SST-INs (Figure 2A). Optical (op)-EPSCs from MDT terminals displayed a trend toward larger amplitudes relative to those from BLA terminals onto SST-INs (Figures 2B and 2C). The GluA2-lacking calcium permeable (CP)-AMPA receptor antagonist NASPM inhibited BLA op-EPSCs onto SST-INs to a greater extent than MDT op-EPSCs (Figure 2D), suggesting that BLA and MDT synapses onto SST-INs differ with respect to AMPA receptor stoichiometry. BLA op-EPSCs readily underwent LTP following mGlu₅ receptor agonism (Figures 2E–2G). By contrast, MDT-driven op-EPSCs onto SST-INs did not undergo long-term adaptations following DHPG application (Figure 2H). These findings provide compelling evidence of an input-specific relationship between the presence of CP-AMPA receptors and the expression of mGlu₅ receptor LTP.

We next performed whole-cell recordings from PFC pyramidal cells to determine whether mGlu₅ receptor activation enhances feedforward inhibition (Figure 2I). BLA and MDT stimulation reliably evoked action potentials in SST-INs and inhibitory postsynaptic currents (IPSCs) in pyramidal cells, with kinetics consistent with disynaptic transmission (Figure S1). Application of DHPG persistently increased the BLA IPSC-to-EPSC (I/E) ratio (Figures 2J and 2K) without affecting MDT I/E (Figure 2L). Together, these data indicate that mGlu₅ receptor activation on SST-INs may locally tune PFC microcircuits to favor BLA-driven feedforward inhibition over concomitant information from the MDT, a circuit process that we predicted may be involved in the response to a stressful experience.

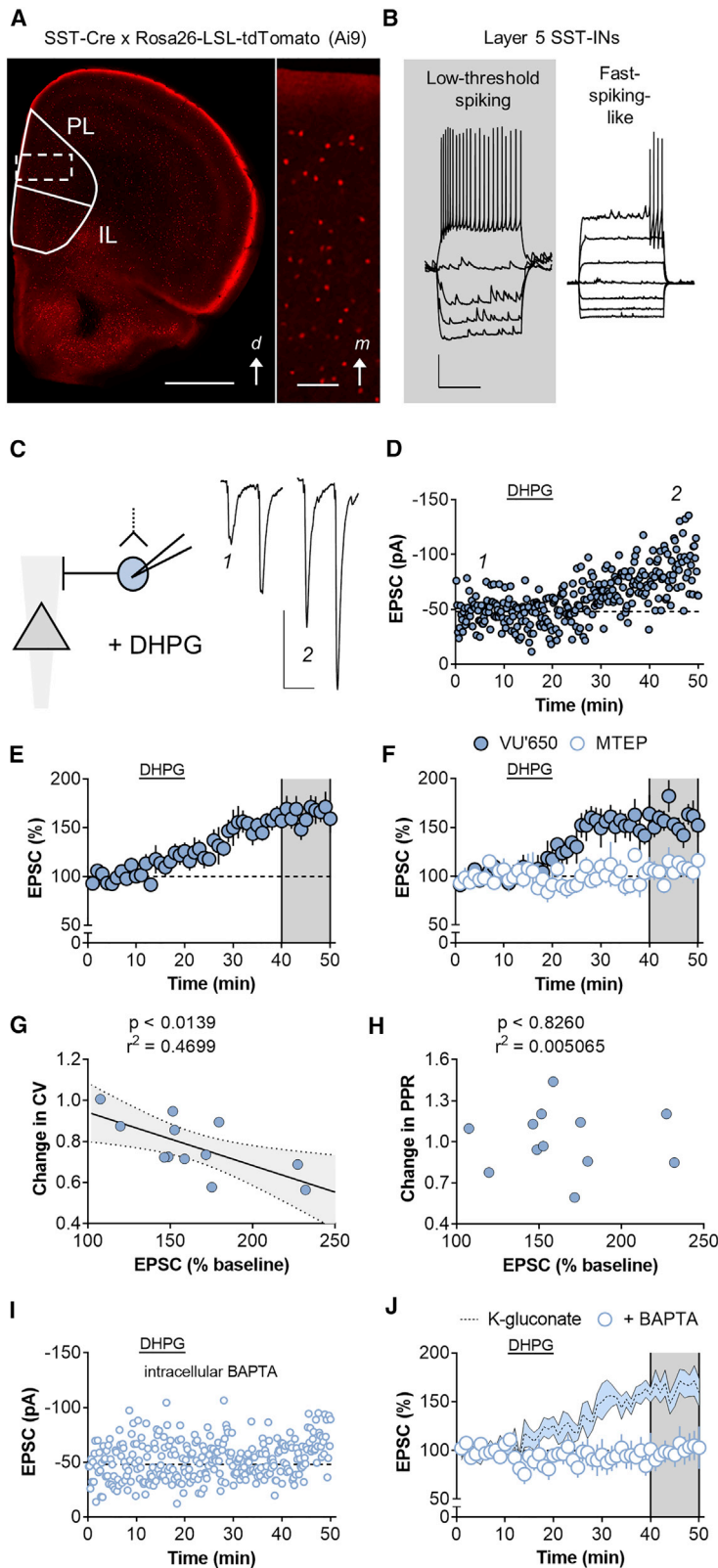


Figure 1. Long-term potentiation (LTP) on prefrontal cortex (PFC) somatostatin interneurons (SST-INs) is regulated by the mGlu₅ metabotropic glutamate receptor

(A) SST-INs were identified via Cre-dependent expression of tdTomato. Left, widefield image of a brain slice displaying tdTomato fluorescence. D, dorsal; PL, prelimbic; IL, infralimbic. Scale bars, 1 mm. Right, digital zoom displaying fluorescent SST-INs throughout all layers. M, medial. Scale bars, 100 μ m.

(B) Whole-cell recordings from identified SST-INs in naive mice. Only low-threshold spiking cells were used for experiments. Scale bars, 20 mV and 500 ms.

(C) Left, excitatory postsynaptic currents (EPSCs) were evoked with local electrical stimulation. Right, representative traces depicting a larger amplitude EPSC following application of the mGlu_{1/5} agonist dihydroxyphenylglycine (DHPG) (100 μ M, 10 min). Scale bars, 50 pA and 50 ms.

(D) Representative time course displaying LTP following DHPG application.

(E) Averaged LTP time course across multiple experiments (146% \pm 11%) n/N = 8/6 cells/mice.

(F) LTP persisted in the presence of the mGlu₁ negative allosteric modulator (NAM) VU0469650 (VU'650) but was blocked by the mGlu₅ NAM MTEP (160% \pm 9% versus 107% \pm 4%; t_{14} = 5.8, p < 0.001, t test). n/N = 8/6.

(G) The magnitude of LTP correlated with the change in the coefficient of variation (CV).

(H) The magnitude of LTP was not associated with a change in the paired-pulse ratio (PPR).

(I) Representative experiment displaying no effect of DHPG when the Ca²⁺ chelator BAPTA is included in the internal solution.

(J) Intracellular BAPTA abrogated LTP (100% \pm 12%; t_{15} = 3.5; p < 0.01, t test versus control). n/N = 5/4. Error bars indicate SEM.

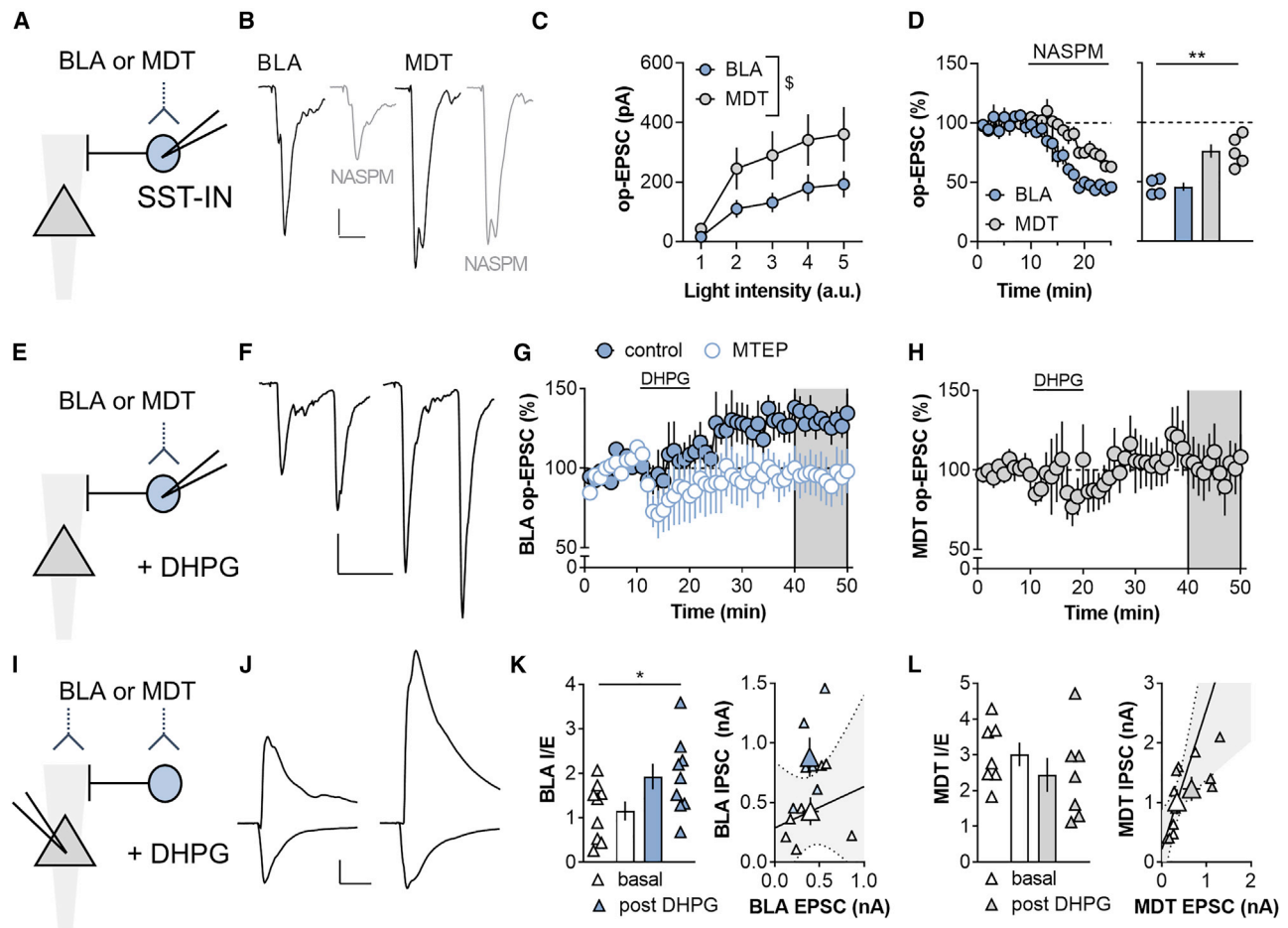


Figure 2. mGlu₅ receptor activation enhances amygdalo-cortical feedforward inhibition

(A) ChR2 was expressed within the basolateral amygdala (BLA) or mediodorsal thalamus (MDT) by viral-mediated gene transfer. Recordings were made from labeled SST-INs and optical (op)-EPSCs were evoked with blue light stimulation.

(B) Representative traces of BLA-PFC op-EPSCs at baseline (black) and after NASPM application (gray). Scale bars, 50 pA and 20 ms.

(C) MDT synapses onto SST-INs displayed a trend toward larger amplitude op-EPSCs relative to BLA inputs (repeated-measures [RM] two-way ANOVA intensity \times input interaction: $F_{4,64} = 2.0$, $p < 0.11$; main effect of intensity: $F_{4,64} = 22.5$, $p < 0.0001$; main effect of input: $F_{1,16} = 3.1$, $p < 0.10$). $n/N = 9/5$ cells/mice per group.

(D) The Ca²⁺-permeable AMPA receptor antagonist NASPM (200 μ M, 15 min) depressed BLA op-EPSCs onto SST-INs to a greater extent than MDT op-EPSCs (46% \pm 4% versus 76% \pm 6%; $t_7 = 4.2$, $p < 0.004$, t test). $n/N = 4-5/4$.

(E) BLA and MDT op-EPSCs onto SST-INs were elicited before during and after application of the mGlu_{1/5} agonist DHPG.

(F) Representative traces of BLA-PFC op-EPSCs at baseline (left) and after DHPG application (right). Scale bars, 100 pA and 50 ms.

(G) The mGlu₅ NAM MTEP blocked LTP of BLA-driven op-EPSCs onto SST-INs (107% \pm 4% versus 160% \pm 9%; $t_{14} = 5.8$, $p < 0.001$, t test). $n/N = 5-8/3-5$.

(H) MDT op-EPSCs did not display LTP (102% \pm 15%). $n/N = 6/3$.

(I) Feedforward inhibition was assessed in pyramidal cells.

(J) Representative traces displaying inward EPSCs evoked at -70 mV and outward inhibitory postsynaptic currents (IPSCs) evoked at 0 mV, at baseline (left) and following DHPG application (right). Scale bars, 200 pA and 50 ms.

(K) DHPG enhanced the BLA IPSC/EPSC (I/E) ratio in pyramidal cells (1.9 \pm 0.3 versus 1.1 \pm 0.2; $t_{16} = 2.16$, $p < 0.05$, t test). $n/N = 9/3$.

(L) DHPG had no effect on the MDT-PFC I/E ratio or either current species in isolation $n/N = 6/3$.

Error bars indicate SEM.

Restraint stress rapidly potentiates excitatory drive from BLA onto PFC SST-Ins

SST-INs are emerging as key mediators in affective behaviors, but our understanding of molecular- and circuit-level adaptations that occur during stressful experiences remains incomplete. To address this gap, we selectively expressed the genetically encoded calcium indicator GcaMP7f in SST-INs and monitored calcium fluctuations during restraint stress using photometry (Fig-

ure 3A). When restrained, mice display struggling episodes characterized by coordinated whole-body movements. We detected these behavioral episodes using an unbiased machine learning tool (Luchsinger et al., 2021; Mathis et al., 2018) and aligned the processed GCaMP7f signals to these events. We found that the onset of struggling episodes coincided with an increase in calcium-dependent GCaMP signals (465 nm) in SST-INs (Figure 3B). Strikingly, the behavior-locked signals increased in magnitude

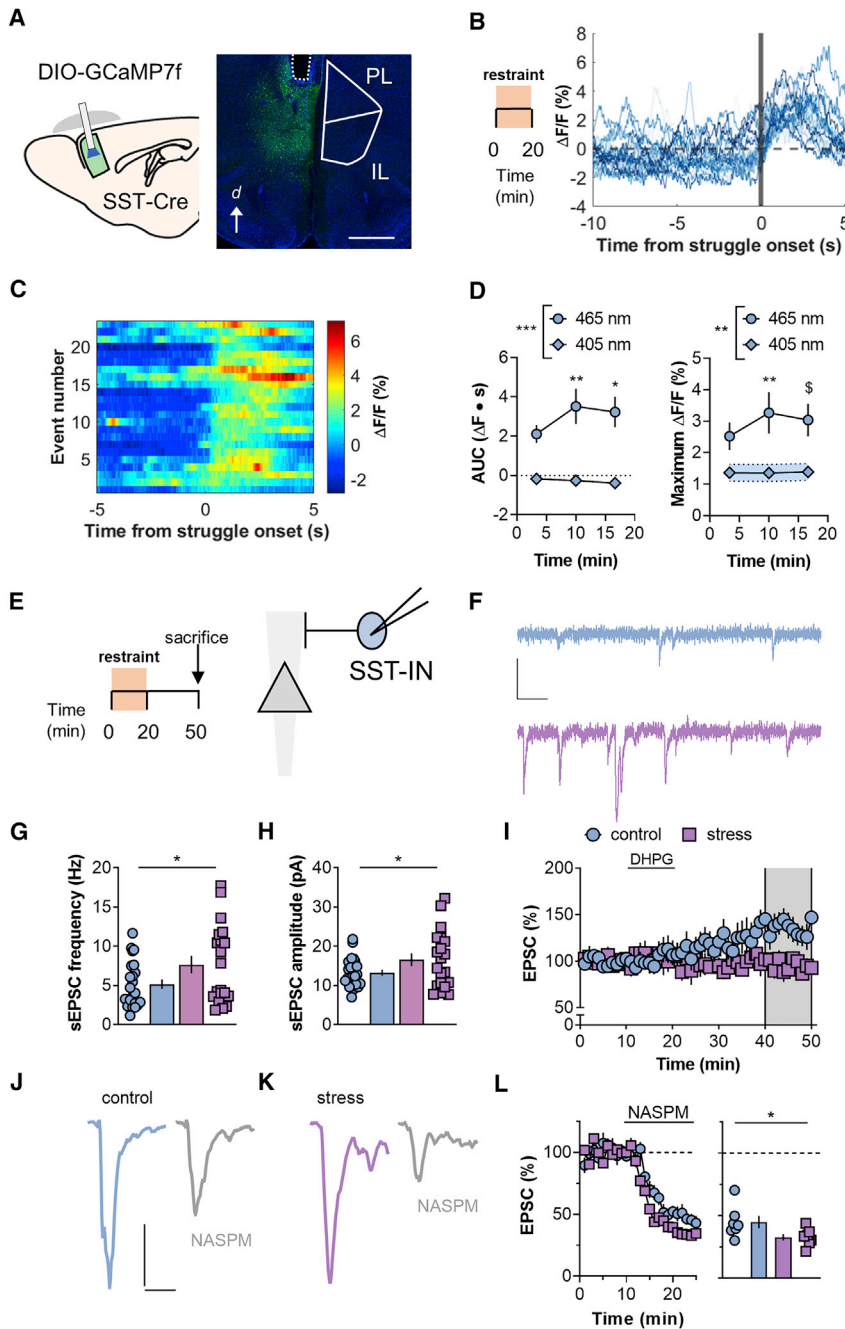


Figure 3. Excitatory drive onto PFC SST-INs is rapidly potentiated during acute stress

(A) Left, schematic displaying viral-assisted approach to express GCaMP7f in SST-INs. A virus promoting the expression of a double-inverted open (DIO) reading frame of GCaMP7f was delivered to the PFC of SST-Cre mice. Chronically indwelling fiberoptic cannulas were implanted. Right, representative image displaying fiber tract (dotted line) and GCaMP expression in PFC SST-INs. D, dorsal; PL, prelimbic; IL, infralimbic. Scale bars, 1 μ m.

(B) After 4 weeks of recovery, animals underwent 20 min restraint stress while SST-IN calcium mobilization was measured via fiber photometry. Representative experiment displaying SST-IN calcium mobilization occurring immediately following behavioral struggling episodes.

(C) Heatmap of representative experiment. Each row denotes SST-GCaMP signal aligned to a behavioral event in chronological order.

(D) Binned data over multiple subjects. Left, the area under the curve (AUC) of the event-locked SST-GCaMP Ca^{2+} -dependent signal (465 nm) increased during a single exposure to restraint stress (RM two-way ANOVA time \times wavelength interaction: $F_{2,16} = 4.3$, $p < 0.04$; main effect of wavelength: $F_{1,8} = 22.7$, $p < 0.001$; $*: p < 0.05$, $**: p < 0.01$ versus Bin 1, Sidak test, $N = 9$ mice). Fluorescent signals on the Ca^{2+} -independent isobestic control channel (405 nm) were not readily detected following struggling episodes. Right, restraint stress potentiated the maximum increase in SST-GCaMP7f fluorescence locked to struggling episodes without altering the isobestic control channel (RM two-way ANOVA time \times wavelength interaction: $F_{2,16} = 3.2$, $p < 0.08$; main effect of wavelength: $F_{1,8} = 11.9$, $p < 0.001$; $\$: p < 0.06$, $**: p < 0.01$ versus Bin 1, Sidak test, $N = 9$).

(E) Mice were sacrificed for whole-cell electrophysiology 30 min following restraint stress. Recordings were made from SST-INs with soma in layer 5 PFC.

(F) Representative traces depicting SST-IN spontaneous EPSCs (sEPSCs) from a control mouse (top, blue) and a mouse that experienced restraint stress (bottom, purple). Scale bars, 20 pA and 50 ms.

(G) Restraint stress rapidly increased sEPSC frequency (7.7 ± 1.1 versus 5.1 ± 0.6 Hz; $t_{41} = 2.1$, $*: p < 0.05$, t test). $n/N = 20\text{--}23/6\text{--}9$.

(H) sEPSC amplitude was greater in SST-INs from the restraint group (16.6 ± 1.6 versus 12.9 ± 0.7 pA; $t_{41} = 2.19$, $*: p < 0.05$, t test). $n/N = 20\text{--}23/6\text{--}9$.

(I) Restraint stress disrupted mGlu₅ receptor LTP ($95\% \pm 7\%$ versus $131\% \pm 11\%$; $t_{16} = 2.49$, $*: p < 0.05$, t test). $n/N = 7\text{--}11/5\text{--}9$.

(J and K) Representative traces displaying SST-INs EPSCs before and after NASPM.

(L) Summarized time course and average of last 5 min of NASPM experiments. SST-IN EPSCs displayed greater sensitivity to NASPM in animals that experienced restraint stress ($33\% \pm 3\%$ versus $45\% \pm 5\%$; $t_{12} = 2.2$, $p < 0.05$, t test). $n/N = 7/5$. Error bars indicate SEM.

over the course of a single restraint stress session (Figures 3C and 3D). Appreciable signals related to the struggling episodes were not detected on the calcium-independent control channel (405 nm). The maximum amplitude of the SST-IN calcium-dependent GCaMP signal also increased over the course of restraint stress. By contrast, interneurons expressing parvalbumin (PV-INs) displayed no adaptations during or immediately following stress (Figure S2).

We next examined how stress regulates SST-IN electrophysiology (Figure 3E). SST-INs from stressed mice were not different from controls with respect to current-evoked spiking or other membrane properties (Figure S3), suggesting that SST-IN potentiation during restraint stress is unlikely to be related to intrinsic physiology. By contrast, excitatory synaptic drive onto SST-INs underwent a rapid increase in strength following restraint stress (Figure 3F). SST-INs from the restraint stress group displayed greater spontaneous excitatory postsynaptic current (sEPSC) frequency (Figure 3G) and amplitude (Figure 3H), consistent with enhanced postsynaptic strength and an increase in the number of detectable synapses. Furthermore, cells from restraint stress mice did not express mGlu₅ receptor-dependent LTP (Figure 3I), suggesting the plasticity may be occluded by restraint stress-induced SST-IN potentiation. Importantly, in agreement with previous observations (Maksymetz et al., 2021; Sun and Neugebauer, 2011), activation of mGlu₁ receptors rapidly increased excitatory drive onto SST-INs, and this phenomenon was not modulated by restraint stress (Figure S3). We also assessed AMPA receptor stoichiometry and found that SST-IN EPSCs from restraint stress mice displayed greater sensitivity to NASPM relative to the control group (Figures 3J–3L).

These findings suggest that restraint stress increases expression of SST-IN GluA2-lacking AMPA receptors and/or potentiates the contribution of BLA op-EPSCs to electrical EPSCs. To address the latter possibility, we examined BLA synapses onto SST-INs from restraint stress mice and controls (Figure 4A). Although BLA op-EPSC amplitude was not different between groups (Figure 4B), we thought of the possibility that changes at specific synaptic loci could occur following restraint stress. We therefore proceeded to perform a multiple probability fluctuation analysis (MPFA) to assess quantal size (Q), synapse number (N), and release probability (P) (Silver, 2003; Suska et al., 2013; Figure 4C). We systematically varied the duration of light stimulation for each SST-IN (Figure 4D). In most cells, the relationship between the variance and amplitude could be fit to an inverse parabola, and Q, N, and P (1 ms) were then extracted from the best fit equation. We validated this method by recording BLA op-EPSCs on SST-INs before and after NASPM application (Figure S4). Strikingly, BLA synapses from SST-INs in the restraint stress group displayed a selective increase in Q relative to controls (Figure 4E). Differences in neither N nor P reached significance between groups (Figures 4F and 4G), and the PPR was not affected by restraint stress (Figure 4H). Collectively, these data are consistent with a mechanism in which restraint stress potentiates excitatory drive from BLA synapses onto PFC SST-INs through mGlu₅ receptor plasticity. We next aimed to assess how restraint stress alters microcircuit function across multiple interacting elements.

BLA inputs recruit SST-INs to shunt MDT-PFC transmission

BLA-driven feedforward inhibition within PFC (Floresco and Tse, 2007; Ji et al., 2010; Pérez-Jaranay and Vives, 1991) can inhibit coincidental information from other long-range excitatory afferents (Dilgen et al., 2013; Esmaeili and Grace, 2013; Ishikawa and Nakamura, 2003; Tejeda and O'Donnell, 2014). We modeled this heterosynaptic interaction by optogenetically stimulating BLA inputs prior to electrical stimulation of superficial layer 1 (Figure 5A), designed to preferentially capture MDT inputs that target pyramidal cell apical dendrites (Collins et al., 2018; Lambe and Aghajanian, 2003; Liu and Aghajanian, 2008). BLA prepulses delivered 3–10 ms prior to electrical stimulation dramatically decreased the amplitude of layer 1-evoked EPSCs (Figure 5B). At the 10 ms interstimulus interval (ISI), consistent with the kinetics for disynaptic transmission (Figure S1), the decreased EPSC amplitude was blocked by including the GABA_A receptor antagonist picrotoxin (PTX) in the patch pipette (Figure 5C).

Although similar phenomena have been described, it remains unclear whether any distinct interneuron population mediates heterosynaptic plasticity in PFC. To address this, we used drugs acutely restricted by tethering (DART) (Shields et al., 2017) to selectively inhibit AMPA receptors on SST-INs (Figure 4D). DART works by genetically programming cells to capture and concentrate a drug to levels ~1,000-fold higher than the ambient concentration, restricting drug action to the experimentally chosen cells. We infected SST-INs with either an active DART virus, featuring a functional HaloTag protein (HT+), or a matched control virus, featuring an inactive mutant HaloTag protein (HT–). We then bath applied the AMPA receptor antagonist, YM90K-DART, at low ambient concentrations that drove rapid capture and EPSC inhibition on HT+ SST-INs without affecting HT– cells (Figure 5E). Because of the covalent nature of DART capture, tethered YM90K-DART persistently attenuated sEPSCs following washout (Figure 5F). Unlike previous studies in striatal medium spiny neurons (Shields et al., 2017), YM90K-DART did not completely block EPSCs on SST-INs, potentially related to partial agonist activity of certain AMPA receptor antagonists at CP-AMPA receptors (Menuz et al., 2007). Nonetheless, YM90K-DART did not affect the PPR or sEPSC frequency (Figure S5), consistent with specific effects on postsynaptic Q in HT+ cells. Inhibiting SST-IN AMPA receptors also attenuated BLA feedforward inhibition on pyramidal cells (Figure S5). Having validated the utility and selectivity of DART in PFC SST-INs, we next tested that phasic excitation of SST-INs is required for BLA-driven disynaptic inhibition (Figure 5G). Under basal conditions, pyramidal cells from mice with HT+ SST-INs readily displayed disynaptic inhibition; however, the interaction was blocked following application of YM90K-DART (Figures 5H and 5I). Although heterosynaptic inhibition at shorter timescales may be mediated by alternative interneuron subtypes, SST-INs appear to be the predominant broker of BLA-mediated disynaptic inhibition within PFC.

We next implemented a dual opsin approach to test whether BLA-mediated feedforward inhibition can impact isolated MDT terminals, by expressing the red-shifted opsin Chrimson in the BLA and ChR2 in the MDT (Figure 5J). As observed with respect to Layer 1-evoked EPSCs, previous stimulation of BLA terminals

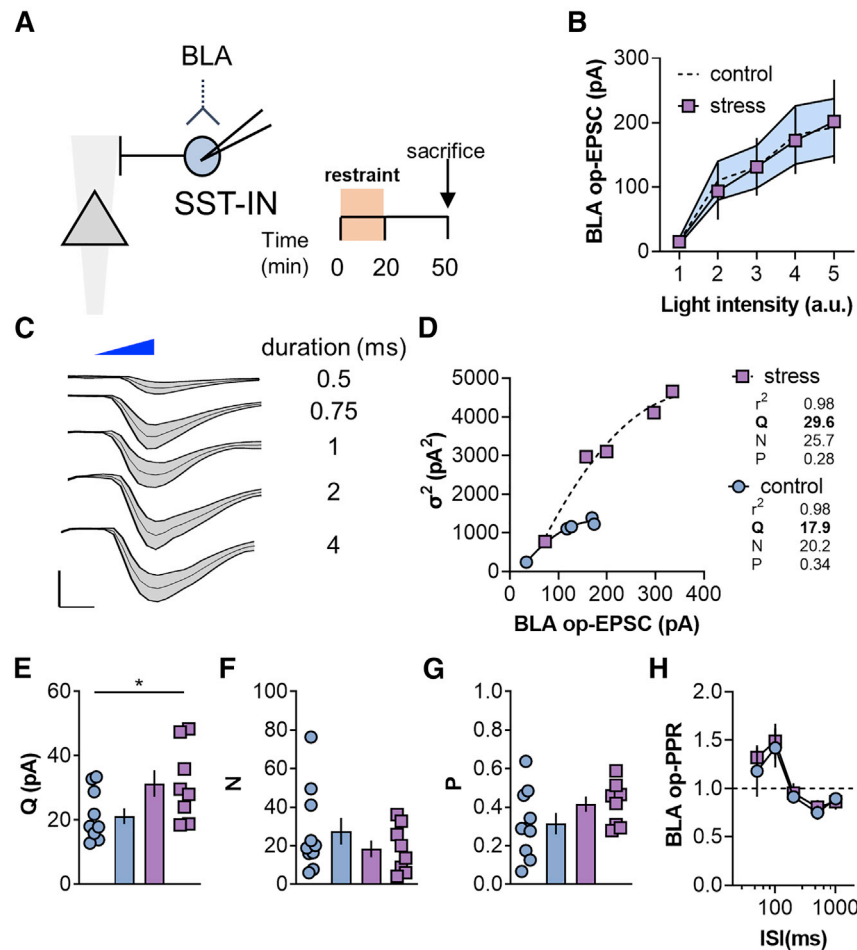


Figure 4. Restraint stress increases postsynaptic strength at BLA inputs onto SST-Ins

(A) BLA op-EPSCs on SST-Ins were collected in control mice and following restraint stress. (B) No difference in BLA op-EPSC amplitude in SST-Ins from control versus stress mice. Control data also presented in Figure 2C. (C) Representative traces displaying BLA op-EPSC amplitude and standard deviation (σ) across a range of light stimulation durations. Scale bars, 100 pA and 2 ms. (D) Representative multiple probability fluctuation analysis (MPFA) experiments. For each SST-IN, a quadratic equation was fit to the op-EPSC amplitude and variance (σ^2). The quantal size (Q), number of synapses (N), and glutamate release probability (P) can be derived from the curve fit parameters. (E) Restraint stress increased Q at BLA synapses on SST-Ins (31.3 ± 4.1 versus 21.2 ± 2.4 pA; $t_{16} = 2.2$, $p < 0.05$, t test). n/N = 8–10/4 cells/mice. (F) Restraint stress did not affect the N at BLA inputs onto SST-Ins. (G) P from BLA to SST-Ins was not affected by restraint stress. (H) BLA op-EPSC PPR was not different on SST-Ins from control versus stress groups. n/N = 7–8/3. Error bars indicate SEM.

attenuated MDT op-EPSCs at short latencies (Figure 5K). Important control experiments demonstrated that BLA-MDT heterosynaptic inhibition exhibits specific directionality, that this effect cannot be attributed to spectral overlap of Chrimson and ChR2, and that GABA_A receptor agonism can attenuate MDT-EPSCs through shunting inhibition (Figure S6). Furthermore, local application of picrotoxin abolished BLA-MDT disinaptic inhibition (Figure 5K). Because the DART pharmacology studies revealed that excitatory synapses on SST-Ins are essential for disinaptic inhibition and restraint stress enhanced excitatory drive onto SST-Ins, we predicted that restraint would disrupt BLA-MDT disinaptic inhibition. Indeed, pyramidal cells did not display BLA-MDT disinaptic inhibition following restraint stress (Figure 5L), suggesting an occluded or otherwise impaired mechanism of action.

Restraint stress enhances BLA-PFC feedforward inhibition

To examine whether restraint stress occludes or impairs feedforward inhibition, we isolated inhibitory synapses on PFC pyramidal cells (Figure 6A). Restraint stress increased inhibitory tone onto pyramidal cells (Figures 6B and 6C). Furthermore, pyramidal cells from stressed mice displayed increased BLA I/E ratios relative to controls (Figures 6D–6F). Stress did not affect the

amplitude of asynchronous (as)-EPSCs (Figure 6G) or the EPSC PPR (Figure 6H), suggesting unaltered physiology of BLA excitatory synapses onto pyramidal cells. We examined MDT-PFC transmission in parallel (Figures 6I and 6J). No effect on the MDT-PFC I/E ratio was observed (Figure 6K), indicating that restraint stress differentially augments feedforward inhibition across subcortical afferents to PFC. In addition, restraint stress decreased the amplitude of MDT-PFC asEPSCs (Figure 6L) without affecting op-EPSC PPR (Figure 6M). Finally, we isolated monosynaptic transmission from SST-Ins to pyramidal cells and found that restraint stress did not affect SST op-IPSCs or PPR (Figures 6N–6Q). Together, this constellation of adaptations suggests that restraint stress selectively increases BLA-PFC feedforward inhibition to facilitate and occlude heterosynaptic inhibition of MDT-PFC transmission. Our previous mechanistic studies raised the possibility that mGlu₅ receptor signaling mediates these circuit-level modifications, and we implemented a genetic approach to test this hypothesis.

Genetic ablation of mGlu₅ receptors from SST-Ins abrogates stress-induced adaptations to PFC physiology

We bred mice to selectively ablate mGlu₅ receptors from SST-Ins via Cre-mediated *Gm5* recombination. In WT mice, approximately 60% of PFC SST-Ins and PV-Ins coexpressed *Gm5* transcript above the threshold of detection (Figures 7A and 7B). By contrast, SST-mGlu₅^{-/-} mice displayed marked reductions of *Gm5* co-expression with *Sst*, without any noticeable change in the proportion of *Pvalb* cells that expressed *Gm5*. The number

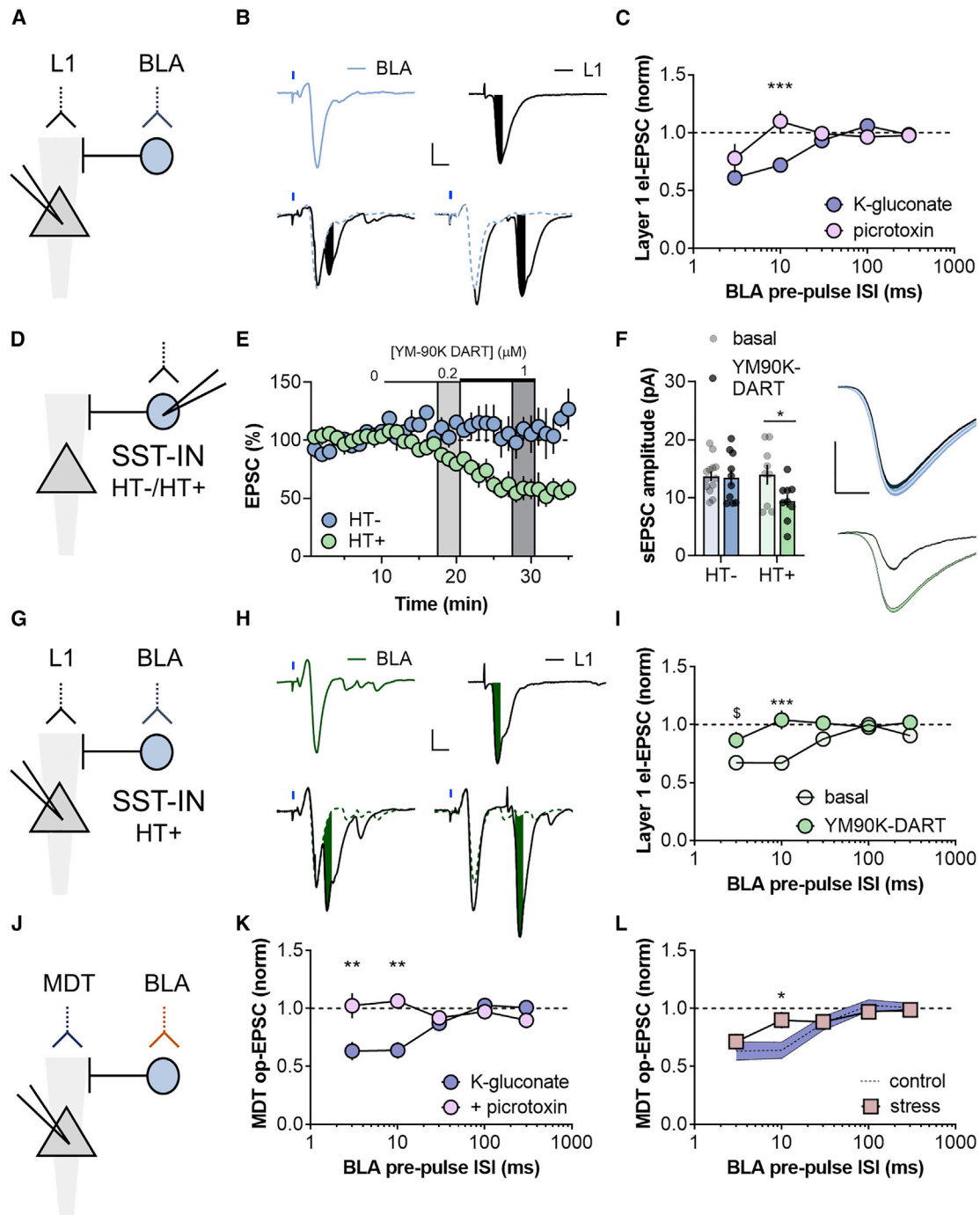


Figure 5. BLA inputs recruit SST-INs to shunt MDT-PFC transmission

(A) Chr2 was expressed in the BLA and electrical (el)-EPSCs were evoked by stimulating distal synapses in layer 1 (L1).

(B) Top, representative traces depicting BLA op-EPSCs and L1 el-EPSCs evoked in the same pyramidal cell. Bottom, recent prior stimulation of BLA terminals inhibited the amplitude of subsequent el-EPSCs (10 ms ISI, left; 30 ms ISI, right). Scale bars, 100 pA and 10 ms.

(C) At short pre-pulse interstimulus intervals (ISIs), BLA terminal stimulation inhibits the amplitude of L1 el-EPSCs. Including the GABA_A receptor antagonist picrotoxin in the patch pipette blocked the effect at the 10 ms disynaptic ISI (RM two-way ANOVA ISI × picrotoxin interaction: $F_{4,60} = 4.4$, $p < 0.01$; ****: $p < 0.001$, Sidak test, $n/N = 8-9/4$ cells/mice).

(D) Drugs acutely restricted by tethering (DART) were deployed by viral-mediated expression of the HaloTag protein (HT+) or an inactive mutant variant (HT-), selectively in PFC SST-INs. Both constructs also expressed tdTomato to allow for visualization and cellular targeting.

(legend continued on next page)

of *Grm5* puncta per cell was also selectively decreased in SST-INs and not PV-INs in SST-mGlu₅^{-/-} mice (Figure 6C). We then used whole-cell electrophysiology to test that postsynaptic receptors mediate LTP on SST-INs. Although normal LTP was observed in controls, DHPG did not affect evoked EPSCs on SST-INs from SST-mGlu₅^{-/-} mice (Figure 7D). Importantly, the agonist-induced increase in sEPSC frequency—an mGlu₁-dependent effect (Figure S3; Maksymetz et al., 2021)—was intact in SST-mGlu₅^{-/-} mice (Figure 7E), suggesting selective alterations to mGlu₅ receptor signaling pathways.

We next tested whether SST-IN mGlu₅ receptor signaling is required for stress-induced adaptations to PFC inhibitory microcircuit function (Figure 7F). We readily detected calcium fluctuations in SST-INs in SST-mGlu₅^{-/-} mice. To our surprise, the area under the curve (AUC) (Figure 7G) and amplitude (Figure 7H) of these events increased during restraint stress, similar to observations in WT mice. These data indicate that the increase in SST-IN calcium signals during acute stress is not a readout of LTP. Nonetheless, if mGlu₅ receptor-dependent signaling is critical for restraint stress-induced plasticity, one would predict that SST-mGlu₅^{-/-} mice would not display typical adaptations in synaptic physiology following restraint. Indeed, although SST-mGlu₅^{-/-} mice displayed enhanced basal excitatory drive relative to WT mice, restraint stress did not increase, and in fact decreased, SST-IN sEPSC frequency in SST-mGlu₅^{-/-} mice as in matched controls (Figures 7I and 7J). In addition, we found that restraint stress rapidly increased spontaneous inhibitory postsynaptic current (sIPSC) frequency in WT mice but not in SST-mGlu₅^{-/-} mice (Figures 7K and 7L). Therefore, although calcium transients in SST-INs during struggling bouts do not directly reflect LTP or mGlu₅ receptor function, the calcium mobilization appears to permit subsequent mGlu₅ receptor plasticity and alterations to PFC microcircuit function. Based on this, we reasoned that SST-IN mGlu₅ receptor signaling may mediate behavioral adaptations following restraint stress.

SST-mGlu₅^{-/-} mice display specific alterations in learning and memory processes related to stress exposure

We first examined restraint stress effects on working memory using a spatial navigation task (Figure 8A). Acute stress, and other manipulations that disrupt working memory, decreases a ro-

dent's ability to successfully alternate through the three distinct arms of a Y-maze (e.g., ABC, not ABA) (Bats et al., 2001; Kim et al., 2018; Ohgidani et al., 2016). Although WT mice displayed impaired spatial alternation following restraint stress, performance in littermate SST-mGlu₅^{-/-} mice was not affected (Figure 8B). No differences were detected in overall locomotion within the Y-maze or behaviors in an open field or an elevated zero-maze (Figure S7), suggesting that SST-IN mGlu₅ receptor signaling is important for conveying physiological adaptations following restraint stress, rather than basal exploration or generalized anxiety. We next examined motivational adaptations following restraint stress. Previous studies have shown that restraint stress and PFC lesions can each decrease operant responding for palatable food on a progressive ratio schedule of reinforcement (Gourley et al., 2010; Joffe et al., 2019). Here, we observed comparable behavior in SST-mGlu₅^{-/-} mice (Figure 7C), indicating that stress-induced SST-IN mGlu₅ receptor plasticity may not affect motivational circuits and/or food-seeking behavior.

Recent studies have also revealed that PFC SST-IN activity is required for associative learning under stressful conditions involving aversive stimuli (Cummings and Clem, 2020; Xu et al., 2019). Furthermore, Cummings and Clem identified potentiation of excitatory transmission onto SST-INs as a key response related to fear learning. Although the molecular mechanisms initiating SST-IN plasticity were not been described in detail, the current findings led us to posit that mGlu₅ receptor signaling is involved in fear learning, predicting that SST-mGlu₅^{-/-} mice would exhibit decreased freezing behavior following cued fear conditioning. Indeed, SST-mGlu₅^{-/-} mice displayed decreased fear learning (Figures 8D and 8E), implicating SST-IN mGlu₅ receptor signaling in aversive associative learning. Based on this, SST-mGlu₅^{-/-} mice displaying impairments in all forms of associative learning or, alternatively, may display selective deficits in learning related to aversive stimuli. To address these two possibilities, we trained mice to self-administer sucrose in an operant discrimination task. WT and SST-mGlu₅^{-/-} mice showed similar rates of discrimination learning (Figure 8F). Taken together, these findings suggest that mGlu₅ receptor signaling on SST-INs is important for a discrete set of behavioral adaptations related to cognitive behaviors following stressful experiences.

(E) The AMPA receptor antagonist YM90K DART dose-dependently inhibited EPSCs on SST-INs following expression of HT+ but not HT- (RM Two-way ANOVA YM90K × HaloTag interaction: $F_{2,14} = 7.2$, $p < 0.01$; main effect of YM90K: $F_{1,7} = 11.4$, $p < 0.05$; 56 ± 9 versus $109\% \pm 12\%$ (1 μ M), $^{*}p < 0.05$, Sidak test). $n/N = 4-5/3-4$.

(F) Following YM90K DART washout, HT+ SST-INs displayed decreased sEPSC amplitude (two-way ANOVA YM90K × HaloTag interaction: $F_{1,37} = 2.9$, $p < 0.1$; $^{*}p < 0.04$, Sidak test). $n/N = 9-13/3-4$. Scale bars, 5 pA and 2 ms.

(G) HT+ was expressed in PFC SST-INs, and ChR2 was expressed in the BLA to evaluate heterosynaptic inhibition of L1 terminals.

(H) Representative recordings showing isolated (top) and summated (bottom) EPSCs following YM-90 K DART application (10 ms ISI, left; 30 ms ISI, right). Scale bars, 100 pA and 10 ms.

(I) SST-IN-directed YM90K-DART blocked BLA-driven heterosynaptic inhibition of EPSCs evoked by L1 stimulation (RM two-way ANOVA ISI × YM90K interaction: $F_{4,36} = 3.1$, $p < 0.03$; $^{***}p < 0.001$; $^{§}p < 0.1$, Sidak test). $n/N = 5-6/3$.

(J) The red-shifted opsin Chrimson was expressed in the BLA, and ChR2 was expressed in the MDT. Red light stimulation preceded blue light stimulation to mitigate concerns related to spectral overlap (see Figure S5).

(K) At short pre-pulse ISIs, BLA stimulation inhibited MDT op-EPSCs in control conditions but not if picrotoxin was included in the patch pipette (two-way ANOVA picrotoxin × ISI interaction: $F_{4,72} = 5.7$, $p < 0.001$; $^{**}p < 0.01$, Sidak test). $n/N = 5-16/2-5$.

(L) A single exposure to 20 min restraint stress disrupted disinhibitory inhibition from the BLA to MDT input to PFC (RM two-way ANOVA stress × ISI: $F_{4,92} = 2.5$, $p < 0.05$; $^{*}p < 0.04$, Sidak test). $n/N = 10-16/3-5$.

Error bars indicate SEM.

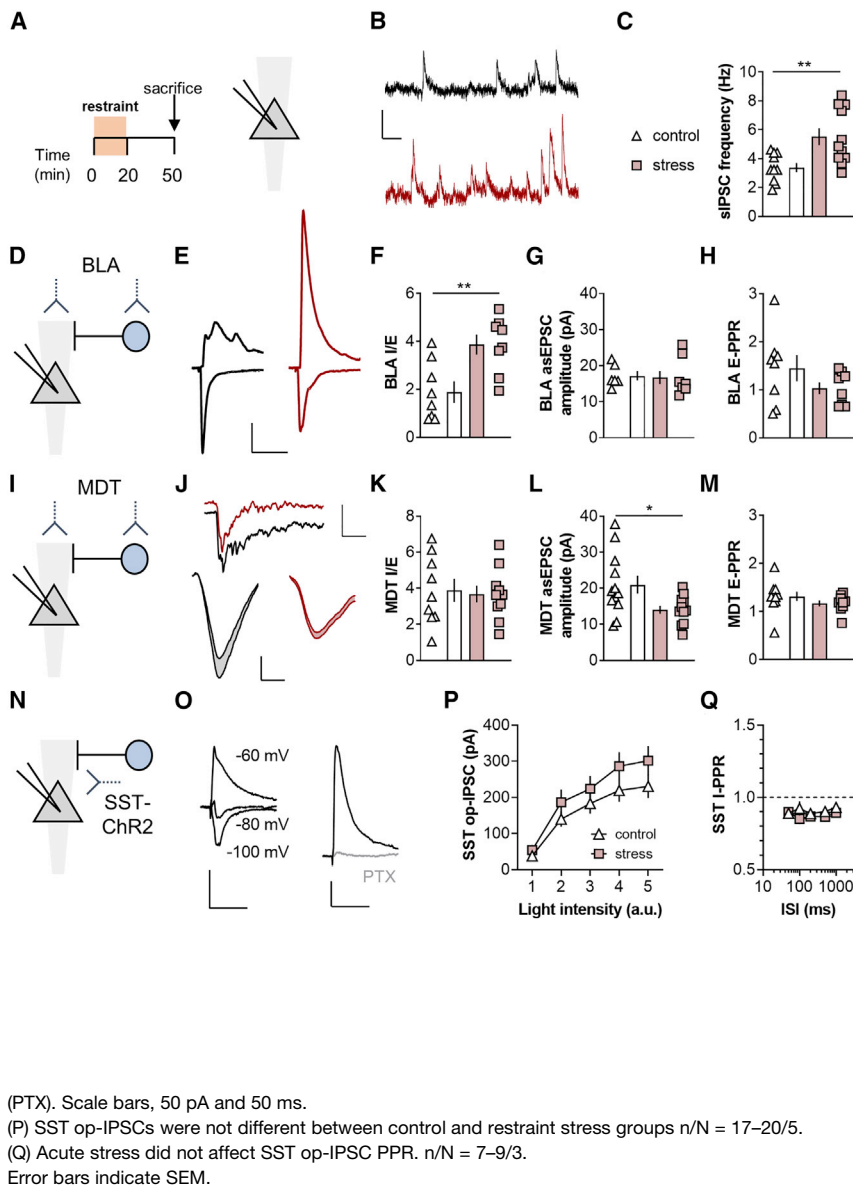


Figure 6. Restraint stress enhances BLA-PFC feedforward inhibition

(A) Recordings were made from layer 5 PL pyramidal cells in mice that experienced restraint stress and controls.
(B) Representative spontaneous inhibitory postsynaptic currents (sIPSCs) from a control mouse (top, black) and one that underwent restraint stress (bottom, red). Scale bars, 10 pA and 100 ms.
(C) Acute stress increased sIPSC frequency ($5.5\% \pm 0.6\%$ versus $3.4\% \pm 0.3\%$; $t_{19} = 3.16$; $**p < 0.01$, t test). $n/N = 10-11/3-4$ cells/mice.
(D) BLA-driven EPSCs and disynaptic IPSCs were elicited using viral-assisted optogenetics.
(E) Representative traces displaying EPSC and IPSC recordings from the control (left, black) and stress (right, red) groups. Scale bars, 100 pA and 50 ms.
(F) Acute stress increased BLA I/E. (3.9 ± 0.4 versus 1.9 ± 0.4 ; $t_{14} = 3.24$; $**p < 0.01$, t test). $n/N = 8/3$.
(G) Acute stress did not affect the amplitude of BLA-driven asynchronous EPSCs (asEPSCs) evoked in strontium-containing ACSF. $n/N = 6-8/3$.
(H) Acute stress did not affect BLA EPSC paired-pulse ratio (E-PPR). $n/N = 8/3$.
(I) Chr2 was expressed in the MDT.
(J) Top, representative traces displaying asEPSCs from representative SST-INs from control (black) and stress (red) groups. Scale bars, 100 pA and 50 ms. Bottom, averaged asEPSCs from representative SST-INs from control (left, black) and restraint stress (right, red) groups. Scale bars, 5 pA and 2 ms.
(K) Restraint stress did not affect MDT I/E ratio. $n/N = 9-10/3$.
(L) Restraint stress decreased MDT asEPSC amplitude (15.0 ± 1.4 versus 21.0 ± 2.5 pA; $t_{23} = 2.13$; $*p < 0.05$, t test). $n/N = 12-13/4$.
(M) Acute stress did not affect MDT E-PPR. $n/N = 9-11/3$.
(N) Chr2 was expressed in SST-INs and recordings were made from pyramidal cells.
(O) SST-driven op-IPSCs displayed a reversal potential near -80 mV and were blocked by picrotoxin

DISCUSSION

Developing a more detailed understanding of the mechanisms by which microcircuit perturbations influence experience-dependent behavioral adaptations is critical for understanding responses to stress and other environmental changes. Here, we report that restraint stress rapidly potentiates excitatory drive onto SST-INs. Our studies collectively suggest that this process occurs through mGlu₅-dependent LTP at BLA inputs to PFC SST-INs, facilitating heterosynaptic inhibition of MDT-PFC transmission. Furthermore, studies using cell-type-specific transgenic mice suggest that these molecular adaptations on SST-INs are necessary for restraint stress-induced changes to PFC physiology and working memory.

The current studies provide a molecular and circuit mechanism relevant for the growing literature indicating that PFC

SST-INs regulate affective behaviors (Ali et al., 2020; Cichon et al., 2017; Cummings and Clem, 2020; Fogaça et al., 2021; Scheggia et al., 2020; Soumier and Sibille, 2014; Xu et al., 2019) and that disease-relevant experiences alter SST-IN synaptic physiology in preclinical models (Cummings and Clem, 2020; Joffe et al., 2020b; Jones and Sheets, 2020). In particular, our findings fit well with recent studies by Cummings and Clem (2020), who observed potentiated excitatory synapses onto PFC SST-INs after fear learning. Interestingly, SST-IN potentiation was not observed in the yoked group that received the noxious unconditioned stimulus without learning the conditioned association. This specific finding could be considered at odds with the present results because we did not implement restraint stress to intentionally form conditioned associations. Nonetheless, it is possible that mice in the present studies readily made associations between the stressful stimuli and the

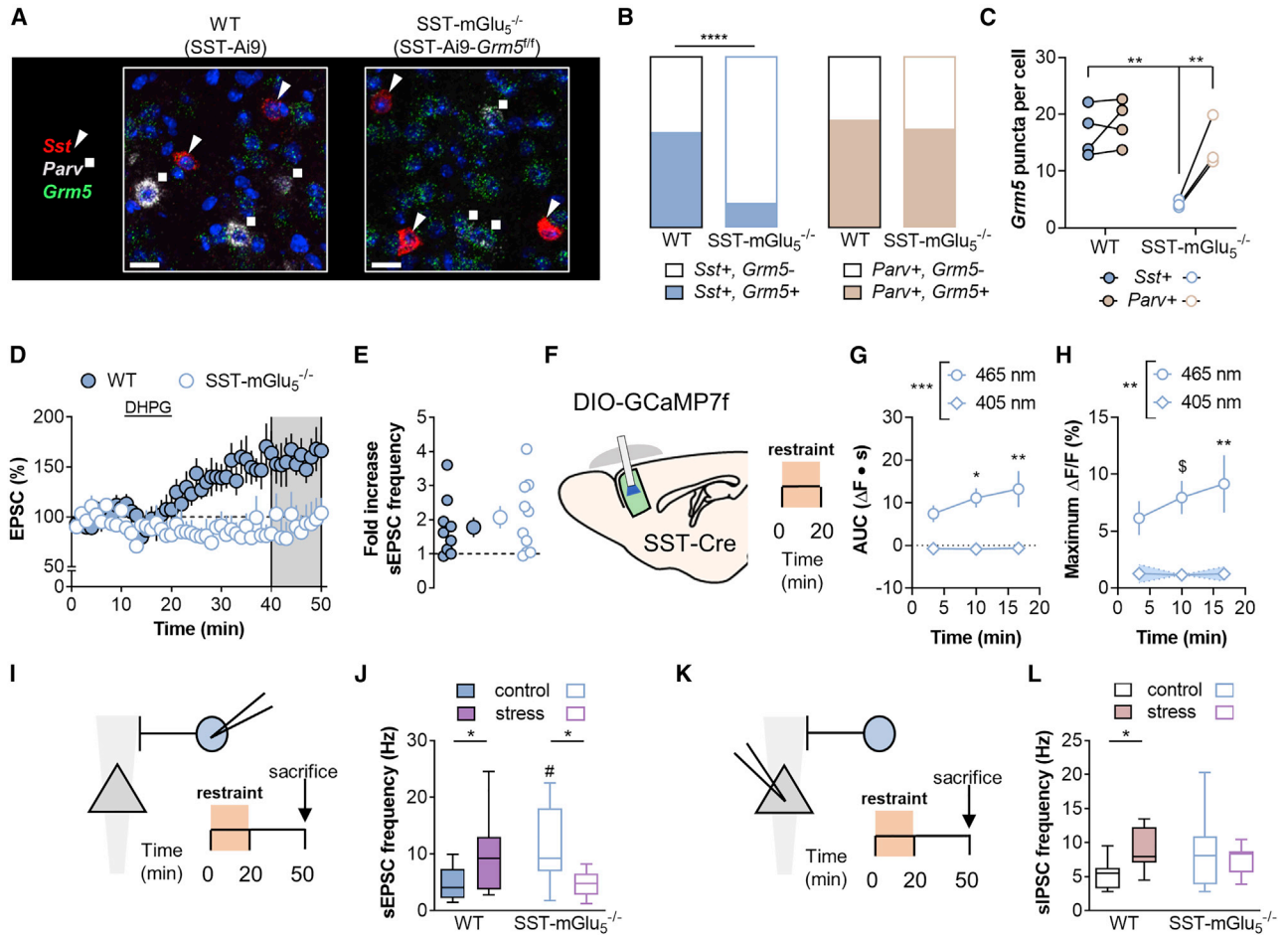


Figure 7. Genetic ablation of mGlu₅ receptors from SST-expressing cells abrogates restraint stress-induced adaptations to PFC physiology

(A) Mice harboring a floxed *Grm5* gene were bred with those expressing Cre recombinase in SST-expressing cells. Representative images displaying cell-type-specific *Grm5* transcript (green) co-expression with *Sst* (red/triangles) and *Parv* (white/squares) was evaluated using RNAscope fluorescent *in situ* hybridization. Scale bars, 20 μ m.

(B) *Grm5* co-expression with *Sst* (left, blue) and *Pvalb* (right, orange) in PFC. The proportion of cells co-expressing *Grm5* with *Sst* was altered in SST-mGlu₅^{-/-} mice ($p < 0.0001$ Fisher's exact test). $n/N = 97\text{--}238/3\text{--}4$ cells/mice.

(C) The number of *Grm5* puncta per cell was reduced in *Sst*-expressing cells in SST-mGlu₅^{-/-} mice (RM two-way ANOVA cell type \times KO interaction: $F_{1,5} = 9.7$, $p < 0.03$; $^{**}p < 0.01$, Sidak test). $N = 3\text{--}4$.

(D) SST-IN recordings were made from WT (filled circles) and SST-mGlu₅^{-/-} mice (open circles). DHPG application induced LTP in SST-INs from control WT mice but not SST-mGlu₅^{-/-} mice. ($159\% \pm 17\%$ versus $91\% \pm 19\%$; $t_9 = 2.67$, $^{*}p < 0.05$, t test). $n/N = 5\text{--}6/3$.

(E) DHPG increased sEPSC frequency on SST-INs comparably in WT and mGlu₅^{-/-} mice. $n/N = 9\text{--}10/5\text{--}6$.

(F) SST-mGlu₅^{-/-} mice underwent 20 min restraint stress while SST-IN calcium mobilization was measured via fiber photometry.

(G) The AUC of the SST-GCaMP Ca^{2+} -dependent signal (465 nm) following struggle bouts increased during restraint stress (RM two-way ANOVA time \times wavelength interaction: $F_{2,16} = 3.8$, $p < 0.05$; main effect of wavelength: $F_{1,8} = 17.1$, $p < 0.004$; $^{*}p < 0.05$, $^{**}p < 0.01$ versus Bin 1, Sidak test, $N = 5$).

(H) Restraint stress potentiated the maximum increase in SST-GCaMP7f fluorescence locked to struggling (RM two-way ANOVA time \times wavelength interaction: $F_{2,16} = 3.7$, $p < 0.05$; main effect of wavelength: $F_{1,8} = 13.3$, $p < 0.007$; $\$p < 0.08$, $^{**}p < 0.01$ versus Bin 1, Sidak test, $N = 5$).

(I) SST-IN recordings were made from WT and SST-mGlu₅^{-/-} mice under control conditions and following restraint stress.

(J) Restraint stress increased sEPSC frequency on SST-INs in control mice (two-way ANOVA stress \times KO: $F_{1,38} = 15.8$, $p < 0.001$; $^{*}p < 0.05$, Sidak test). sEPSC frequency on SST-INs from SST-mGlu₅^{-/-} mice was enhanced relative to WT controls and decreased following acute stress ($\#p < 0.01$ Sidak test versus WT; $^{*}p < 0.05$, Sidak test). $n/N = 8\text{--}12/3$.

(K) Pyramidal cell recordings were made from WT and SST-mGlu₅^{-/-} mice under control conditions and following restraint stress.

(L) Acute stress increased sIPSC frequency in control mice but not SST-mGlu₅^{-/-} mice (two-way ANOVA stress \times KO: $F_{1,39} = 5.3$, $p < 0.03$; $^{*}p < 0.05$, Sidak test). $n/N = 10\text{--}11/3\text{--}4$.

Error bars indicate SEM. Box plots indicate median, interquartile range, and range.

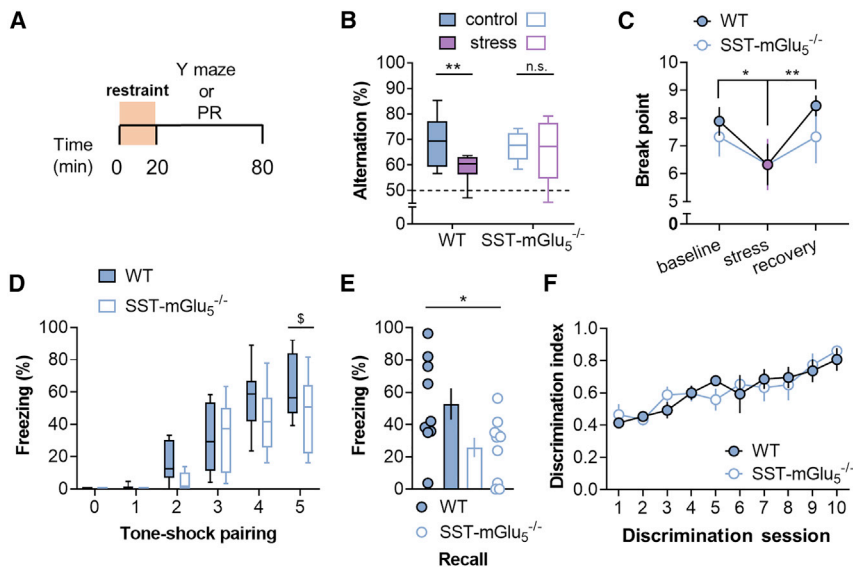


Figure 8. SST-mGlu₅^{-/-} mice display specific alterations in cognitive behaviors

(A) Mice underwent 20 min acute restraint stress immediately prior to testing cognitive and motivational behaviors.

(B) In control mice, stress decreased the percent of correct alternations in the Y-maze task. SST-mGlu₅^{-/-} mice displayed normal performance under control conditions and were not impaired by acute stress (two-way ANOVA stress × KO interaction: $F_{1,38} = 2.5$, $p < 0.12$; main effect of stress: $F_{1,38} = 6.1$, $p < 0.02$; $^*p < 0.02$, Sidak test) $N = 10$ –12 mice.

(C) Mice performed holepokes in an operant chamber to obtain liquid food reinforcement on a progressive ratio schedule. Acute restraint stress decreased the number of rewards earned, but no effect of genotype or interaction was observed. (RM two-way ANOVA stress × KO interaction: $F_{2,26} = 0.9$, n.s.; main effect of stress: $F_{2,26} = 7.6$, $p < 0.01$; $^*p < 0.02$, $^{**}p < 0.01$ Sidak test.) $N = 6$ –9.

(D) SST-mGlu₅^{-/-} mice trended toward decreased tone-related freezing on the conditioning day. (RM two-way ANOVA tone × KO interaction: $F_{5,85} = 1.9$, $p < 0.1$; main effect of KO: $F_{1,17} = 2.7$, $p < 0.12$; $§p < 0.053$, Sidak test.) $N = 9$ –10.

(E) 1 day after conditioning, SST-mGlu₅^{-/-} mice

displayed decreased recall of cued freezing. ($25.9\% \pm 6.0\%$ versus $52.8\% \pm 9.7\%$; $t_{17} = 2.41$; $^*p < 0.03$, t test). $N = 9$ –10.

(F) WT and SST-mGlu₅^{-/-} mice did not differ in performance during an operant discrimination task reinforced by sucrose delivery (RM two-way ANOVA session × KO interaction: $F_{9,81} = 1.0$, n.s.; main effect of KO: $F_{1,9} < 0.01$, n.s.). $N = 5$ –6.

Error bars indicate SEM. Box plots indicate median, interquartile range, and range.

apparatus or other environmental factors. A potential alternative explanation relates to the time course of stress-induced adaptations. All recordings made by Cummings and Clem (2020) occurred 1 day following the presentation of noxious stimuli, whereas the present study assessed adaptations that occur during or immediately after restraint. Based on this, the LTP mechanism described here may provide an initial, permissive step allowing for associations or other adaptations to be encoded within a subsequent critical window of plasticity.

Another factor that could contribute to differences between these and other studies examining PFC SST-INs is their decided heterogeneity. Neocortical SST-INs can be subdivided into no less than 4 and up to 100 subtypes based on distribution, molecular identity, and function (Tremblay et al., 2016; Urban-Ciecko and Barth, 2016; Yavorska and Wehr, 2016). Although the *ex vivo* experiments herein were restricted to SST-INs exhibiting a low-threshold spiking phenotype, the inability for SST-Cre tools to discern between these SST-IN subpopulations is a clear limitation to the present *in vivo* studies. By extension, another important caveat is the basal increase in excitatory drive and calcium fluctuations in SST-mGlu₅^{-/-} mice, a finding that we believe is likely related to alterations to mGlu₁ receptor function (Maksymetz et al., 2021) and/or changes in glutamate-driven SST-IN development (Tuncdemir et al., 2016). These baseline changes could have contributed to the observation that restraint stress “decreased” excitatory drive onto SST-INs in mGlu₅^{-/-} mice. Future studies should leverage emerging technologies harnessing combinatorial genetics and new viral approaches to manipulate specific interneuron subpopulations at discrete time points.

Here, we show that restraint stress increases excitatory drive onto PFC SST-INs and inhibition onto pyramidal cells. Despite

these dynamic changes in synaptic transmission, we found no evidence for persistent alterations in the membrane properties of SST-INs. Similarly, we and others have found no persistent effect of acute stress on pyramidal cell membrane properties in *ex vivo* studies (Joffe et al., 2019; Varela et al., 2012). However, pyramidal cells are a heterogeneous group of neurons that project to various cortical and subcortical structures (Gabbott et al., 2005; Sesack et al., 1989) and exhibit various firing patterns in response to acute stress *in vivo* (Jackson and Moghaddam, 2006). Considering that distinct PFC outputs can differentially regulate cognitive and motivated behaviors (Diehl et al., 2020; Halladay et al., 2020; Jayachandran et al., 2019; Jenni et al., 2017; Otis et al., 2017), future studies should address whether acute stress differentially affects membrane physiology and feedforward inhibition onto one or more subsets of the pyramidal cell. Pyramidal cells that project to different structures vary with respect to their excitatory inputs. The present studies showed that BLA-driven feedforward inhibition can potently depress MDT op-EPSCs, and previous work has demonstrated that BLA inputs can similarly inhibit transmission from the ventral hippocampus (VH) (Esmaili and Grace, 2013; Ishikawa and Nakamura, 2003; Tejeda and O'Donnell, 2014). These findings raise the possibility that acute stress may preferentially alter SST-IN inhibition onto neurons that receive large inputs from the MDT and/or VH, namely cortico-cortical pyramidal cells (Collins et al., 2018; Liu and Carter, 2018). This appealing hypothesis is consistent with our finding that SST-mGlu₅^{-/-} mice resisted stress-induced disruptions in spatial alternation, considering that MDT inputs, VH inputs, and recurrent cortico-cortical circuits have all been associated with working memory (Abbas et al., 2018; Bolkan

et al., 2017; Spellman et al., 2015). Future studies should examine additional sources of glutamate, notably intracortical connections, and whether similar or alternative mechanisms regulate SST-IN function in other prefrontal regions responsive to acute stress, including the cingulate, infralimbic, and orbitofrontal cortices.

We used cell-type-directed DART pharmacology to demonstrate that phasic excitatory transmission proceeds through SST-INs to inhibit EPSCs on nearby pyramidal cells. This finding is especially interesting, considering that excitatory synapses on SST-INs generally display low glutamate release probability and SST-IN activity is thought to emerge primarily during repetitive barrages of activity (Beierlein et al., 2003; González-Burgos et al., 2004; Kapfer et al., 2007; McGarry and Carter, 2016). In addition to the effects on phasic inhibition, the current studies suggest that restraint stress may amplify tonic SST-IN activity, as assessed by increased sIPSC frequency on pyramidal cells. Spontaneous SST-IN activity *in vivo* can regulate pyramidal cells through GABA_B receptors (Gentet et al., 2012; Urban-Ciecko and Barth, 2016; Urban-Ciecko et al., 2015), and this signaling merits examination in the context of stress and other disease-relevant experiences. Furthermore, many studies suggest that stress-induced potentiation of SST-IN function is likely to inhibit calcium mobilization and long-term plasticity on PFC pyramidal cells (Ali et al., 2020; Gentet et al., 2012; Marlin and Carter, 2014). SST-IN synapses on pyramidal cells are enriched with $\alpha 5$ -containing GABA_A receptors, which can inhibit NMDA receptor function, action potential back-propagation, and spike-timing-dependent plasticity (Groen et al., 2014; Schulz et al., 2018). Thus, in addition to altering heterosynaptic interactions following phasic fast transmission, stress-induced increases in BLA-SST-IN feedforward inhibition are likely to have important long-term ramifications for synaptic plasticity on pyramidal cells. An intriguing hypothesis for future studies is that persistent SST-IN signaling during chronic stress exposure can lead to pyramidal cell dendritic retraction, spine loss, anhedonia, and other depressive-like behaviors. Future studies examining SST-IN adaptations in multiple stress models will be of interest from a basic neurobiology perspective and to inform efforts to develop modulators of mGlu₅ receptors, NMDA receptors, GABA_B receptors, and $\alpha 5$ -containing GABA_A receptors as psychiatric disease treatments.

STAR★METHODS

Detailed methods are provided in the online version of this paper and include the following:

- KEY RESOURCES TABLE
- RESOURCE AVAILABILITY
 - Lead contact
 - Materials availability
 - Data and code availability
- EXPERIMENTAL MODEL AND SUBJECT DETAILS
 - Mice
- METHOD DETAILS
 - Restraint stress
 - Viral-assisted gene transfer

- Fiberoptic cannulations
- Electrophysiology
- DART
- RNA scope fluorescence-based *in situ* hybridization
- Open field
- Elevated zero-maze
- Y maze
- Progressive ratio
- Fear conditioning
- Operant discrimination
- Fiber photometry

● QUANTIFICATION AND STATISTICAL ANALYSIS

SUPPLEMENTAL INFORMATION

Supplemental information can be found online at <https://doi.org/10.1016/j.neuron.2021.12.027>.

ACKNOWLEDGMENTS

The authors thank members of the Vanderbilt WCND and VCAR and the UPMC TNP for stimulating and formative discussions. Initial breeders for the *Grm5^{fl/fl}* mouse colony were generously provided by Margarita Behrens. Research was supported by the National Institutes of Health grants R01MH062646 and R37NS031373 to P.J.C., R37AA019455 and R01DA042475 to D.G.W., RF1MH117055 and DP2MH119425 to M.R.T., F30AA027126 to J.R.L., R00DA045103 to C.A.S., and R00DA042111 and DP1DA048931 to E.S.C. M.E.J. was supported by K99/R00AA027806 and a postdoctoral fellowship through the Pharmaceutical Research and Manufacturers of America Foundation. J.M. was supported by the Vanderbilt International Scholars Program and the Canadian Institutes for Health Research Doctoral Foreign Study Award DFS146189. E.S.C. and C.A.S. were supported by funds from the Brain and Behavior Research Foundation. E.S.C. was supported by funds from the Whitehall Foundation and the Edward Mallinckrodt, Jr. Foundation. C.A.S. was supported by an independent grant program sponsored by Alkermes Pharmaceuticals. The authors thank the William K. Warren Foundation for endowing the WCND. Some experiments were performed using the Vanderbilt University Medical Center Murine Neurobehavior Core and Cell Imaging Shared Resource. The graphical abstract was created with BioRender.com.

AUTHOR CONTRIBUTIONS

Conceptualization: M.E.J.; investigation: M.E.J., J.M., J.R.L., S.D., A.S.F., D.J.L., I.M.G., Z.X., H.B., and P.R.M.; methodology: M.E.J., J.M., J.L.L., K.M.W., S.W.C., and E.S.C.; resources: B.C.S., C.W.L., and M.R.T.; supervision: M.E.J., C.A.S., C.M.N., D.G.W., and P.J.C.; writing—original draft: M.E.J.; writing—review and editing: all authors.

DECLARATION OF INTERESTS

P.J.C., C.W.L., and C.M.N. receive research support from Acadia Pharmaceuticals and Boehringer Ingelheim, and C.W.L. also receives support from Ono Pharmaceutical. P.J.C., C.W.L., and C.M.N. are inventors on multiple patents for allosteric modulators of metabotropic glutamate receptors. All other authors declare no potential conflicts of interest.

INCLUSION AND DIVERSITY

We worked to ensure sex balance in the selection of non-human subjects. One or more of the authors of this paper self-identifies as an underrepresented ethnic minority in science. One or more of the authors of this paper self-identifies as a member of the LGBTQ+ community. One or more of the authors of this paper self-identifies as living with a disability. One or more of the authors of this paper received support from a program designed to increase minority

representation in science. While citing references scientifically relevant for this work, we also actively worked to promote gender balance in our reference list.

Received: April 8, 2021

Revised: November 10, 2021

Accepted: December 17, 2021

Published: January 19, 2022

REFERENCES

- Abbas, A.I., Sundiang, M.J.M., Henoeh, B., Morton, M.P., Bolkan, S.S., Park, A.J., Harris, A.Z., Kellendonk, C., and Gordon, J.A. (2018). Somatostatin interneurons facilitate hippocampal-prefrontal synchrony and prefrontal spatial encoding. *Neuron* *100*, 926–939.e3.
- Akam, T., and Walton, M.E. (2019). pyPhotometry: open source Python based hardware and software for fiber photometry data acquisition. *Sci. Rep.* *9*, 3521.
- Ali, F., Gerhard, D.M., Sweasy, K., Pothula, S., Pittenger, C., Duman, R.S., and Kwan, A.C. (2020). Ketamine disinhibits dendrites and enhances calcium signals in prefrontal dendritic spines. *Nat. Commun.* *11*, 72.
- Bats, S., Thoumas, J.L., Lordi, B., Tonon, M.C., Lalonde, R., and Caston, J. (2001). The effects of a mild stressor on spontaneous alternation in mice. *Behav. Brain Res.* *118*, 11–15.
- Beierlein, M., Gibson, J.R., and Connors, B.W. (2003). Two dynamically distinct inhibitory networks in layer 4 of the neocortex. *J. Neurophysiol.* *90*, 2987–3000.
- Bolkan, S.S., Stujenske, J.M., Parnaudeau, S., Spellman, T.J., Rauffenbart, C., Abbas, A.I., Harris, A.Z., Gordon, J.A., and Kellendonk, C. (2017). Thalamic projections sustain prefrontal activity during working memory maintenance. *Nat. Neurosci.* *20*, 987–996.
- Cichon, J., Blanck, T.J.J., Gan, W.B., and Yang, G. (2017). Activation of cortical somatostatin interneurons prevents the development of neuropathic pain. *Nat. Neurosci.* *20*, 1122–1132.
- Collins, D.P., Anastasiades, P.G., Marlin, J.J., and Carter, A.G. (2018). Reciprocal circuits linking the prefrontal cortex with dorsal and ventral thalamic nuclei. *Neuron* *98*, 366–379.e4.
- Cummings, K.A., and Clem, R.L. (2020). Prefrontal somatostatin interneurons encode fear memory. *Nat. Neurosci.* *23*, 61–74.
- Dana, H., Sun, Y., Mohar, B., Hulse, B.K., Kerlin, A.M., Hasseman, J.P., Tsegaye, G., Tsang, A., Wong, A., Patel, R., et al. (2019). High-performance calcium sensors for imaging activity in neuronal populations and microcompartments. *Nat. Methods* *16*, 649–657.
- Diehl, M.M., Iravedra-Garcia, J.M., Morán-Sierra, J., Rojas-Bowe, G., Gonzalez-Diaz, F.N., Valentin-Valentin, V.P., and Quirk, G.J. (2020). Divergent projections of the prelimbic cortex bidirectionally regulate active avoidance. *Elife* *9*, e59281.
- Dilgen, J., Tejada, H.A., and O'Donnell, P. (2013). Amygdala inputs drive feed-forward inhibition in the medial prefrontal cortex. *J. Neurophysiol.* *110*, 221–229.
- Dogra, S., Stansley, B.J., Xiang, Z., Qian, W., Gogliotti, R.G., Nicoletti, F., Lindsley, C.W., Niswender, C.M., Joffe, M.E., and Conn, P.J. (2021). Activating mGlu3 metabotropic glutamate receptors rescues schizophrenia-like cognitive deficits through metaplastic adaptations within the hippocampus. *Biol. Psychiatry* *90*, 385–398.
- Duman, R.S., Aghajanian, G.K., Sanacora, G., and Krystal, J.H. (2016). Synaptic plasticity and depression: new insights from stress and rapid-acting antidepressants. *Nat. Med.* *22*, 238–249.
- Esmaili, B., and Grace, A.A. (2013). Afferent drive of medial prefrontal cortex by hippocampus and amygdala is altered in MAM-treated rats: evidence for interneuron dysfunction. *Neuropsychopharmacology* *38*, 1871–1880.
- Floresco, S.B., and Tse, M.T. (2007). Dopaminergic regulation of inhibitory and excitatory transmission in the basolateral amygdala-prefrontal cortical pathway. *J. Neurosci.* *27*, 2045–2057.
- Fogaça, M.V., and Duman, R.S. (2019). Cortical GABAergic dysfunction in stress and depression: new insights for therapeutic interventions. *Front. Cell. Neurosci.* *13*, 87.
- Fogaça, M.V., Wu, M., Li, C., Li, X.Y., Picciotto, M.R., and Duman, R.S. (2021). Inhibition of GABA interneurons in the mPFC is sufficient and necessary for rapid antidepressant responses. *Mol. Psychiatry* *26*, 3277–3291.
- Gabbott, P.L., Warner, T.A., Jays, P.R., Salway, P., and Busby, S.J. (2005). Prefrontal cortex in the rat: projections to subcortical autonomic, motor, and limbic centers. *J. Comp. Neurol.* *492*, 145–177.
- Gentet, L.J., Kremer, Y., Taniguchi, H., Huang, Z.J., Staiger, J.F., and Petersen, C.C. (2012). Unique functional properties of somatostatin-expressing GABAergic neurons in mouse barrel cortex. *Nat. Neurosci.* *15*, 607–612.
- González-Burgos, G., Krimer, L.S., Urban, N.N., Barrionuevo, G., and Lewis, D.A. (2004). Synaptic efficacy during repetitive activation of excitatory inputs in primate dorsolateral prefrontal cortex. *Cereb. Cortex* *14*, 530–542.
- Gould, R.W., Dencker, D., Grannan, M., Bubser, M., Zhan, X., Wess, J., Xiang, Z., Locuson, C., Lindsley, C.W., Conn, P.J., et al. (2015). Role for the M1 muscarinic acetylcholine receptor in top-down cognitive processing using a touchscreen visual discrimination task in mice. *ACS Chem. Neurosci.* *6*, 1683–1695.
- Gourley, S.L., Lee, A.S., Howell, J.L., Pittenger, C., and Taylor, J.R. (2010). Dissociable regulation of instrumental action within mouse prefrontal cortex. *Eur. J. Neurosci.* *32*, 1726–1734.
- Groen, M.R., Paulsen, O., Pérez-Garci, E., Nevia, T., Wortel, J., Dekker, M.P., Mansvelter, H.D., van Ooyen, A., and Meredith, R.M. (2014). Development of dendritic tonic GABAergic inhibition regulates excitability and plasticity in CA1 pyramidal neurons. *J. Neurophysiol.* *112*, 287–299.
- Halladay, L.R., Kocharian, A., Piantadosi, P.T., Authement, M.E., Lieberman, A.G., Spitz, N.A., Coden, K., Glover, L.R., Costa, V.D., Alvarez, V.A., et al. (2020). Prefrontal regulation of punished ethanol self-administration. *Biol. Psychiatry* *87*, 967–978.
- Higley, M.J. (2014). Localized GABAergic inhibition of dendritic Ca(2+) signaling. *Nat. Rev. Neurosci.* *15*, 567–572.
- Hippenmeyer, S., Vrieseling, E., Sigrist, M., Portmann, T., Laengle, C., Ladle, D.R., and Arber, S. (2005). A developmental switch in the response of DRG neurons to ETS transcription factor signaling. *PLoS Biol* *3*, e159.
- Holmes, A., and Wellman, C.L. (2009). Stress-induced prefrontal reorganization and executive dysfunction in rodents. *Neurosci. Biobehav. Rev.* *33*, 773–783.
- Hu, H., Cavendish, J.Z., and Agmon, A. (2013). Not all that glitters is gold: off-target recombination in the somatostatin-IRES-Cre mouse line labels a subset of fast-spiking interneurons. *Front. Neural Circuits* *7*, 195.
- Ishikawa, A., and Nakamura, S. (2003). Convergence and interaction of hippocampal and amygdalar projections within the prefrontal cortex in the rat. *J. Neurosci.* *23*, 9987–9995.
- Jackson, M.E., and Moghaddam, B. (2006). Distinct patterns of plasticity in prefrontal cortex neurons that encode slow and fast responses to stress. *Eur. J. Neurosci.* *24*, 1702–1710.
- Jayachandran, M., Linley, S.B., Schlecht, M., Mahler, S.V., Vertes, R.P., and Allen, T.A. (2019). Prefrontal pathways provide top-down control of memory for sequences of events. *Cell Rep* *28*, 640–654.e6.
- Jenni, N.L., Larkin, J.D., and Floresco, S.B. (2017). Prefrontal dopamine D1 and D2 receptors regulate dissociable aspects of decision making via distinct ventral striatal and amygdalar circuits. *J. Neurosci.* *37*, 6200–6213.
- Ji, G., Sun, H., Fu, Y., Li, Z., Pais-Vieira, M., Galhardo, V., and Neugebauer, V. (2010). Cognitive impairment in pain through amygdala-driven prefrontal cortical deactivation. *J. Neurosci.* *30*, 5451–5464.
- Joffe, M.E., Santiago, C.I., Engers, J.L., Lindsley, C.W., and Conn, P.J. (2019). Metabotropic glutamate receptor subtype 3 gates acute stress-induced dysregulation of amygdalo-cortical function. *Mol. Psychiatry* *24*, 916–927.
- Joffe, M.E., Santiago, C.I., Oliver, K.H., Maksymetz, J., Harris, N.A., Engers, J.L., Lindsley, C.W., Winder, D.G., and Conn, P.J. (2020a). mGlu2 and mGlu3 negative allosteric modulators divergently enhance thalamocortical

- transmission and exert rapid antidepressant-like effects. *Neuron* 105, 46–59.e3.
- Joffe, M.E., Santiago, C.I., Stansley, B.J., Maksymetz, J., Gogliotti, R.G., Engers, J.L., Nicoletti, F., Lindsley, C.W., and Conn, P.J. (2019). Mechanisms underlying prelimbic prefrontal cortex mGlu3/mGlu5-dependent plasticity and reversal learning deficits following acute stress. *Neuropharmacology* 144, 19–28.
- Joffe, M.E., Winder, D.G., and Conn, P.J. (2020b). Contrasting sex-dependent adaptations to synaptic physiology and membrane properties of prefrontal cortex interneuron subtypes in a mouse model of binge drinking. *Neuropharmacology* 178, 108126.
- Jones, A.F., and Sheets, P.L. (2020). Sex-specific disruption of distinct mPFC inhibitory neurons in spared-nerve injury model of neuropathic pain. *Cell Rep* 31, 107729.
- Kapfer, C., Glickfeld, L.L., Atallah, B.V., and Scanziani, M. (2007). Supralinear increase of recurrent inhibition during sparse activity in the somatosensory cortex. *Nat. Neurosci.* 10, 743–753.
- Kim, J.W., Ko, M.J., Gonzales, E.L., Kang, R.J., Kim, D.G., Kim, Y., Seung, H., Oh, H.A., Eun, P.H., and Shin, C.Y. (2018). Social support rescues acute stress-induced cognitive impairments by modulating ERK1/2 phosphorylation in adolescent mice. *Sci. Rep.* 8, 12003.
- Klapoetke, N.C., Murata, Y., Kim, S.S., Pulver, S.R., Birdsey-Benson, A., Cho, Y.K., Morimoto, T.K., Chuong, A.S., Carpenter, E.J., Tian, Z., et al. (2014). Independent optical excitation of distinct neural populations. *Nat. Methods* 11, 338–346.
- Lambe, E.K., and Aghajanian, G.K. (2003). Hypocretin (orexin) induces calcium transients in single spines postsynaptic to identified thalamocortical boutons in prefrontal slice. *Neuron* 40, 139–150.
- Le Duigou, C., and Kullmann, D.M. (2011). Group I mGluR agonist-evoked long-term potentiation in hippocampal oriens interneurons. *J. Neurosci.* 31, 5777–5781.
- Lewis, D.A., Curley, A.A., Glausier, J.R., and Volk, D.W. (2012). Cortical parvalbumin interneurons and cognitive dysfunction in schizophrenia. *Trends Neurosci* 35, 57–67.
- Liston, C., McEwen, B.S., and Casey, B.J. (2009). Psychosocial stress reversibly disrupts prefrontal processing and attentional control. *Proc. Natl. Acad. Sci. USA* 106, 912–917.
- Liu, R.J., and Aghajanian, G.K. (2008). Stress blunts serotonin- and hypocretin-evoked EPSCs in prefrontal cortex: role of corticosterone-mediated apical dendritic atrophy. *Proc. Natl. Acad. Sci. USA* 105, 359–364.
- Liu, X., and Carter, A.G. (2018). Ventral hippocampal inputs preferentially drive corticocortical neurons in the infralimbic prefrontal cortex. *J. Neurosci.* 38, 7351–7363.
- Luchsinger, J.R., Fetterly, T.L., Williford, K.M., Salimando, G.J., Doyle, M.A., Maldonado, J., Simerly, R.B., Winder, D.G., and Centanni, S.W. (2021). Delineation of an insula-BNST circuit engaged by struggling behavior that regulates avoidance in mice. *Nat. Commun.* 12, 3561.
- Luscher, B., Shen, Q., and Sahir, N. (2011). The GABAergic deficit hypothesis of major depressive disorder. *Mol. Psychiatry* 16, 383–406.
- Maksymetz, J., Byun, N.E., Luessen, D.J., Li, B., Barry, R.L., Gore, J.C., Niswender, C.M., Lindsley, C.W., Joffe, M.E., and Conn, P.J. (2021). mGlu1 potentiation enhances prelimbic somatostatin interneuron activity to rescue schizophrenia-like physiological and cognitive deficits. *Cell Rep* 37, 109950.
- Maksymetz, J., Joffe, M.E., Moran, S.P., Stansley, B.J., Li, B., Temple, K., Engers, D.W., Lawrence, J.J., Lindsley, C.W., and Conn, P.J. (2019). M1 muscarinic receptors modulate fear-related inputs to the prefrontal cortex: implications for novel treatments of posttraumatic stress disorder. *Biol. Psychiatry* 85, 989–1000.
- Marlin, J.J., and Carter, A.G. (2014). GABA-A receptor inhibition of local calcium signaling in spines and dendrites. *J. Neurosci.* 34, 15898–15911.
- Mathis, A., Mamidanna, P., Cury, K.M., Abe, T., Murthy, V.N., Mathis, M.W., and Bethge, M. (2018). DeepLabCut: markerless pose estimation of user-defined body parts with deep learning. *Nat. Neurosci.* 21, 1281–1289.
- McBain, C.J., DiChiara, T.J., and Kauer, J.A. (1994). Activation of metabotropic glutamate receptors differentially affects two classes of hippocampal interneurons and potentiates excitatory synaptic transmission. *J. Neurosci.* 14, 4433–4445.
- McEwen, B.S., and Morrison, J.H. (2013). The brain on stress: vulnerability and plasticity of the prefrontal cortex over the life course. *Neuron* 79, 16–29.
- McGarry, L.M., and Carter, A.G. (2016). Inhibitory gating of basolateral amygdala inputs to the prefrontal cortex. *J. Neurosci.* 36, 9391–9406.
- Menuz, K., Stroud, R.M., Nicoll, R.A., and Hays, F.A. (2007). TARP auxiliary subunits switch AMPA receptor antagonists into partial agonists. *Science* 318, 815–817.
- Nath, T., Mathis, A., Chen, A.C., Patel, A., Bethge, M., and Mathis, M.W. (2019). Using DeepLabCut for 3D markerless pose estimation across species and behaviors. *Nat. Protoc.* 14, 2152–2176.
- Nigro, M.J., Hashikawa-Yamasaki, Y., and Rudy, B. (2018). Diversity and connectivity of layer 5 somatostatin-expressing interneurons in the mouse barrel cortex. *J. Neurosci.* 38, 1622–1633.
- Ohgidani, M., Kato, T.A., Sagata, N., Hayakawa, K., Shimokawa, N., Sato-Kasai, M., and Kanba, S. (2016). TNF-alpha from hippocampal microglia induces working memory deficits by acute stress in mice. *Brain Behav. Immun.* 55, 17–24.
- Otis, J.M., Nambodiri, V.M., Matan, A.M., Voets, E.S., Mohorn, E.P., Kosyk, O., McHenry, J.A., Robinson, J.E., Resendez, S.L., Rossi, M.A., et al. (2017). Prefrontal cortex output circuits guide reward seeking through divergent cue encoding. *Nature* 543, 103–107.
- Pelkey, K.A., Chittajallu, R., Craig, M.T., Tricoire, L., Wester, J.C., and McBain, C.J. (2017). Hippocampal GABAergic inhibitory interneurons. *Physiol. Rev.* 97, 1619–1747.
- Perez, Y., Morin, F., and Lacaille, J.C. (2001). A Hebbian form of long-term potentiation dependent on mGluR1a in hippocampal inhibitory interneurons. *Proc. Natl. Acad. Sci. USA* 98, 9401–9406.
- Pérez-Jaranay, J.M., and Vives, F. (1991). Electrophysiological study of the response of medial prefrontal cortex neurons to stimulation of the basolateral nucleus of the amygdala in the rat. *Brain Res* 564, 97–101.
- Prévot, T., and Sibille, E. (2021). Altered GABA-mediated information processing and cognitive dysfunctions in depression and other brain disorders. *Mol. Psychiatry* 26, 151–167.
- R Development Core Team. (2018). R: A language and environment for statistical computing (R Foundation for Statistical Computing).
- Scheggia, D., Managò, F., Maltese, F., Bruni, S., Nigro, M., Dautan, D., Latuske, P., Contarini, G., Gomez-Gonzalo, M., Reque, L.M., et al. (2020). Somatostatin interneurons in the prefrontal cortex control affective state discrimination in mice. *Nat. Neurosci.* 23, 47–60.
- Schulz, J.M., Knoflach, F., Hernandez, M.C., and Bischofberger, J. (2018). Dendrite-targeting interneurons control synaptic NMDA-receptor activation via nonlinear alpha5-GABAA receptors. *Nat. Commun.* 9, 3576.
- Sesack, S.R., Deutch, A.Y., Roth, R.H., and Bunney, B.S. (1989). Topographical organization of the efferent projections of the medial prefrontal cortex in the rat: an anterograde tract-tracing study with Phaseolus vulgaris leucoagglutinin. *J. Comp. Neurol.* 290, 213–242.
- Shields, B.C., Kahuno, E., Kim, C., Apostolides, P.F., Brown, J., Lindo, S., Mensh, B.D., Dudman, J.T., Lavis, L.D., and Tadross, M.R. (2017). Deconstructing behavioral neuropharmacology with cellular specificity. *Science* 356, eaaj2161.
- Silver, R.A. (2003). Estimation of nonuniform quantal parameters with multiple-probability fluctuation analysis: theory, application and limitations. *J. Neurosci. Methods* 130, 127–141.
- Sinha, R., Lacadie, C.M., Constable, R.T., and Seo, D. (2016). Dynamic neural activity during stress signals resilient coping. *Proc. Natl. Acad. Sci. USA* 113, 8837–8842.
- Soares, J.M., Sampaio, A., Ferreira, L.M., Santos, N.C., Marques, F., Palha, J.A., Cerqueira, J.J., and Sousa, N. (2012). Stress-induced changes in human decision-making are reversible. *Transl. Psychiatry* 2, e131.

- Sorge, R.E., Martin, L.J., Isbester, K.A., Sotocinal, S.G., Rosen, S., Tuttle, A.H., Wieskopf, J.S., Acland, E.L., Dokova, A., Kadoura, B., et al. (2014). Olfactory exposure to males, including men, causes stress and related analgesia in rodents. *Nat. Methods* *11*, 629–632.
- Soumier, A., and Sibille, E. (2014). Opposing effects of acute versus chronic blockade of frontal cortex somatostatin-positive inhibitory neurons on behavioral emotionality in mice. *Neuropsychopharmacology* *39*, 2252–2262.
- Spellman, T., Rigotti, M., Ahmari, S.E., Fusi, S., Gogos, J.A., and Gordon, J.A. (2015). Hippocampal-prefrontal input supports spatial encoding in working memory. *Nature* *522*, 309–314.
- Sun, H., and Neugebauer, V. (2011). mGluR1, but not mGluR5, activates feed-forward inhibition in the medial prefrontal cortex to impair decision making. *J. Neurophysiol.* *106*, 960–973.
- Suska, A., Lee, B.R., Huang, Y.H., Dong, Y., and Schlüter, O.M. (2013). Selective presynaptic enhancement of the prefrontal cortex to nucleus accumbens pathway by cocaine. *Proc. Natl. Acad. Sci. USA* *110*, 713–718.
- Taniguchi, H., He, M., Wu, P., Kim, S., Paik, R., Sugino, K., Kvitsiani, D., Fu, Y., Lu, J., Lin, Y., et al. (2011). A resource of Cre driver lines for genetic targeting of GABAergic neurons in cerebral cortex. *Neuron* *71*, 995–1013.
- Tejeda, H.A., and O'Donnell, P. (2014). Amygdala inputs to the prefrontal cortex elicit heterosynaptic suppression of hippocampal inputs. *J. Neurosci.* *34*, 14365–14374.
- Tremblay, R., Lee, S., and Rudy, B. (2016). GABAergic interneurons in the neocortex: from cellular properties to circuits. *Neuron* *91*, 260–292.
- Tuncdemir, S.N., Wamsley, B., Stam, F.J., Osakada, F., Goulding, M., Callaway, E.M., Rudy, B., and Fishell, G. (2016). Early somatostatin interneuron connectivity mediates the maturation of deep layer cortical circuits. *Neuron* *89*, 521–535.
- Urban-Ciecko, J., and Barth, A.L. (2016). Somatostatin-expressing neurons in cortical networks. *Nat. Rev. Neurosci.* *17*, 401–409.
- Urban-Ciecko, J., Fanselow, E.E., and Barth, A.L. (2015). Neocortical somatostatin neurons reversibly silence excitatory transmission via GABAB receptors. *Curr. Biol.* *25*, 722–731.
- Varela, J.A., Wang, J., Christianson, J.P., Maier, S.F., and Cooper, D.C. (2012). Control over stress, but not stress per se increases prefrontal cortical pyramidal neuron excitability. *J. Neurosci.* *32*, 12848–12853.
- Wickham, H., Averick, M., Bryan, J., Chang, W., McGowan, L., François, R., Grolemond, G., Hayes, A., Henry, L., Hester, J., et al. (2019). Welcome to the Tidyverse. *J. Open Source Software* *4*, 1686.
- Xu, H., Liu, L., Tian, Y., Wang, J., Li, J., Zheng, J., Zhao, H., He, M., Xu, T.L., Duan, S., et al. (2019). A disinhibitory microcircuit mediates conditioned social fear in the prefrontal cortex. *Neuron* *102*, 668–682.e5.
- Xu, J., Zhu, Y., Contractor, A., and Heinemann, S.F. (2009). mGluR5 has a critical role in inhibitory learning. *J. Neurosci.* *29*, 3676–3684.
- Yavorska, I., and Wehr, M. (2016). Somatostatin-expressing inhibitory interneurons in cortical circuits. *Front. Neural Circuits* *10*, 76.

STAR★METHODS

KEY RESOURCES TABLE

Reagent or Resource	Source	Identifier
RNAscope <i>in situ</i> Hybridization Probes		
<i>Grm5</i> (target region 2409-3336)	ACDBio	NM_001081414.2
<i>Sst</i> (target region 18-407)	ACDBio	NM_009215.1
<i>Pvalb</i> (target region 2-885)	ACDBio	NM_013645.3
Viruses		
AAV5-hSyn-hChr2(H134R)-EYFP (7e12 vg/mL)	unpublished	RRID:Addgene_26973
AAV5-EF1a-double floxed-hChr2(H134R)-EYFP-WPRE-HGHpA (1e13 vg/mL)	unpublished	RRID:Addgene_20298
AAV5-Syn-ChrimsonR-tdT (7e12 vg/mL)	(Klapeotke et al., 2014)	RRID:Addgene_59171
AAV9-syn-FLEX-jGCaMP7f-WPRE (1e13 vg/mL)	(Dana et al., 2019)	RRID:Addgene_104492
AAV10-CAG-FLEX-HaloTagDART2.0-2A-dTomato-WPRE (2e12 vg/mL)	MR Tadross	N/A
AAV10-CAG-FLEX-ddHaloTagDART2.0-2A-dTomato-WPRE (2e12 vg/mL)	MR Tadross	N/A
Chemicals		
(S)-3,5-DHPG (100 μM)	HelloBio	Cat # HB0045
D-AP5 (50 μM)	Tocris	Cat # 0106
CNQX (20 μM)	Tocris	Cat # 1045
Picrotoxin (1 μM in pipette)	Tocris	Cat # 1128
Muscimol (10 μM)	HelloBio	Cat # HB0887
MTEP (1 μM)	Tocris	Cat # 2921
VU0469650 (10 μM)	Tocris	Cat # 537950
BAPTA (20 mM in pipette)	Sigma	Cat # 14510
NASPM (200 μM)	HelloBio	Cat # HB0441
YM90K-DART_2.0 (0.2 - 1 μM)	MR Tadross	N/A
Alx647-DART_2.0 (0.02 - 0.1 μM)	MR Tadross	N/A
Experimental Models		
Mouse: C57BL/6J	The Jackson Laboratory	000664
Mouse: mGluR5-loxP; B6.129-Grm5tm1.1Jixu/J	The Jackson Laboratory	028626
Mouse: SST Cre; Ssttm2.1(cre)Zjh/J	The Jackson Laboratory	013044
Mouse: PV Cre; B6;129P2-Pvalbtm1(cre)Arbr/J	The Jackson Laboratory	017320
Mouse: Ai9; B6.Cg-Gt(ROSA)26Sortm9(CAG-tdTomato)Hze/J	The Jackson Laboratory	007909
Software and Algorithms		
pClamp	Molecular Devices	RRID:SCR_011323
Prism 8.0	GraphPad Software	RRID:SCR_002798
DeepLabCut 2.1.5	DeepLabCut	https://github.com/AlexEMG/DeepLabCut
MATLAB 2019a	Mathworks	RRID:SCR_001622
Fiber photometry analysis code	custom code	10.5281/zenodo.5777173
Synapse Suite	Tucker-Davis Technologies	https://www.tdt.com/component/synapse-software/

(Continued on next page)

Continued

Reagent or Resource	Source	Identifier
RStudio	RStudio, Inc.	RRID:SCR_000432
R	R Foundation	RRID:SCR_001905
Fiji	NIH	RRID:SCR_002285

RESOURCE AVAILABILITY

Lead contact

Further information and requests for resources and reagents should be directed to and will be fulfilled by the lead contact, Dr. Max Joffe (joffeme@upmc.edu).

Materials availability

New reagents were not developed during these studies.

Data and code availability

- Requests for raw data should be made to and will be fulfilled by the lead contact.
- Code used for fiber photometry analysis has been deposited at Zenodo and is publicly available. The DOI is listed in the key resources table.
- Any additional information required to reanalyze the data reported in this paper is available from the lead contact upon request.

EXPERIMENTAL MODEL AND SUBJECT DETAILS

Mice

Female and male mice were bred and housed 2-5 per cage on a standard 12-hour light cycle (on at 6:00 am). Transgenic mice expressing tdTomato fluorescent protein in PFC interneurons were generated by crossing female SST-IRES-Cre mice ([Taniguchi et al., 2011](#)) (Jackson Laboratories, Stock No: 028864) or PV-Cre mice ([Hippenmeyer et al., 2005](#)) (Jackson Laboratories, Stock No: 017320) with male C57BL/6J mice or Rosa26-loxP-STOP-loxP-CAG-tdTomato “Ai9” mice (Jackson Laboratories, Stock No: 007909). SST-mGlu₅^{-/-} mice were generated with all breeders homozygous for floxed *Grm5* ([Xu et al., 2009](#)) (Jackson Laboratories, Stock No: 028626). All breeding strains were maintained on congenic C57BL/6J genetic backgrounds. Experimental mice were not excluded based on external genitalia. For each type of experiment, the proportion of mouse sex was balanced between treatment groups, although some physiology experimental conditions happened to be limited to only male or female mice. A complete breakdown of mouse sex for electrophysiology experiments can be found in [Table S2](#). All behavioral experiments contained roughly half female mice and half male mice in each group.

METHOD DETAILS

Restraint stress

Acute restraint stress was applied for 20 minutes using custom-made or commercially available acrylic tubes. Throughout all studies, control mice underwent many sensory manipulations in parallel to the mice in the restraint stress group. For electrophysiology studies, all mice were removed from their home cages, placed in a transfer bucket, moved approximately 300 yards to the laboratory, placed in a new room for one hour, and sacrificed under anesthesia. For behavioral studies, all mice were removed from the colony room, transferred to an antechamber for one hour, and then placed in the Y-maze or operant conditioning chamber. Restraint stress terminated 30 minutes prior to animal sacrifice for electrophysiology or immediately prior to behavioral experiments ([Joffe et al., 2019](#)). All physiology experiments were performed in mice at least 8 weeks of age or older. Behavioral experiments were conducted in mice at least 12 weeks of age or older.

Viral-assisted gene transfer

Between 5-16 weeks of age mice underwent stereotaxic viral injections under isoflurane anesthesia as described ([Maksymetz et al., 2019](#)). Chr2 and Chrimson were expressed in all neurons within the BLA and/or MDT via 250-400 nL injections. GCaMP7f and Chr2 were expressed in Cre-expressing neurons within PFC via 400 nL injections. HT+ or its inactive control, HT-, were expressed in Cre-expressing neurons within PFC via 2, 300 nL injections. AAV5-hSyn-hChr2(H134R)-EYFP and AAV5-EF1a-double floxed-hChr2(H134R)-EYFP-WPRE-HGHpA were gifts from Karl Deisseroth (Addgene viral prep # 26973-AAV5 and # 20298-AAV5). AAV5-Syn-ChrimsonR-tdTomato ([Klappoetke et al., 2014](#)) was a gift from Edward Boyden (Addgene viral prep # 59171-AAV5). AAV9-syn-FLEX-jGCaMP7f-WPRE ([Dana et al., 2019](#)) was a gift from Douglas Kim & GENIE Project (Addgene viral prep # 104492-AAV9). AAV10-CAG-FLEX-HaloTagDART2.0-2A-dTomato-WPRE and AAV10-CAG-FLEX-ddHaloTagDART2.0-2A-dTomato-WPRE were prepared by the Duke Viral Vector Core.

Fiberoptic cannulations

During the same procedure to express GCaMP7f within PFC, a chronically indwelling fiberoptic cannula was implanted immediately following virus infusion. A single, 250- μ m core, 0.48 NA, 2-mm length fiberoptic cannula (Doric Lenses) was slowly lowered in PFC and the secured with a base layer of C&B-Metabond epoxy and a surrounding headcap prepared with dental cement (Patterson Dental). Mice were returned to group-housing following fiberoptic cannulation without issue.

Electrophysiology

Acute prelimbic PFC slices were prepared for whole-cell patch-clamp physiology as described (Joffe et al., 2020a, 2020b). Briefly, mice decapitated under isoflurane anesthesia. Brains were removed without perfusion and coronal slices (300 μ m) were immediately prepared in *N*-methyl-D-glucamine (NMDG) solution (in mM): 93 NMDG, 20 HEPES, 2.5 KCl, 0.5 CaCl₂, 10 MgCl₂, 1.2 NaH₂PO₄, 25 glucose, 5 Na-ascorbate, and 3 Na-pyruvate. Slices recovered for 10 minutes in warm (30–32 °C) NMDG solution and were then maintained in room-temperature (22–24 °C) for >1 hour in artificial cerebrospinal fluid (ACSF), containing (in mM): 119 NaCl, 2.5 KCl, 2.5 CaCl₂, 1.3 MgCl₂, 1 NaH₂PO₄, 11 glucose, and 26 NaHCO₃. Cells were then transferred to a recording chamber mounted on an BX51 inverted microscope (Olympus) and superfused with 30–32 °C ACSF at 2 mL/min. ACSF was also used to fill recording electrodes for field potential experiments.

For most studies, membrane physiology and excitatory synaptic physiology were assessed with a potassium-based internal solution (in mM): 125 K-gluconate, 4 NaCl, 10 HEPES, 4 MgATP, 0.3 NaGTP, 10 Tris-phosphocreatine. Cells within layer 5 prelimbic subregion were dialyzed with K-based internal solution for 5 minutes before undergoing a series of current injections to assess intrinsic physiology. Interneuron selection was guided by tdTomato fluorescence. SST-tdTomato neurons with low R_m (<150 M Ω), hyperpolarized V_m (<-75 mV), high rheobase (>100 pA), and high maximal firing frequency (>60 Hz) (Table S1) were immediately discarded, as they represent ectopic tdTomato expression stemming from transient SST expression during development (Hu et al., 2013), or non-Martinotti type SST-INs (Nigro et al., 2018). Pyramidal cells were initially selected by their large soma and prominent apical dendrite. Some cells were excluded for displaying low capacitance, high R_m , and/or non-adaptive spike-firing properties.

Cells were voltage-clamped at -80 mV to electrically isolate excitatory postsynaptic currents (EPSCs). For long-term recordings, electrical and optical EPSCs were evoked with paired pulses (50 ms ISI) at 0.1 Hz using stimulation parameters to elicit EPSCs between 50–600 pA at the onset of experiments. For experiments reporting normalized data, the average and range of responses are found in Table S2. DHPG (100 μ M) was applied in the bath for 10 minutes with concurrent stimulation. Changes in sEPSC frequency were calculated by normalizing the value over the last 5 minutes of drug application to the last 5 minutes of baseline. Asynchronous (as)EPSCs were obtained in a modified ACSF where all supplemental calcium was replaced with equimolar strontium. asEPSCs were analyzed for 200 ms after the peak opEPSC.

The multiple probability fluctuation analysis (MPFA) was based off previous studies (Silver, 2003; Suska et al., 2013). BLA op-EPSCs were collected at interleaved stimulations [0.5,0.75,1,2,4 ms]. Stimulations occurred at 1 Hz and at least 30 responses were analyzed at each stimulation duration for each cell. For each stimulation duration, we plotted the variance (σ^2) of the op-EPSC amplitude versus its peak amplitude. If presynaptic release sites operate independently, and the release probability (P) is not different across synapses contributing to op-EPSCs onto a given cell, the EPSC amplitude (I) can be expressed as the product of P , synapse number (N), and quantal size (Q):

$$I = NPQ$$

Assuming a binomial model, the following equation can be assumed:

$$\sigma^2 = NQ^2P(1 - P)$$

From those equations, the following equation can be reduced:

$$\sigma^2 = IQ - (I^2 / N^2)$$

Based on this, a parabolic relationship resembling an “inverted U” is predicted between σ^2 and I . Indeed, BLA op-EPSCs from most SST-INs were fit well by a second-order polynomial. N and Q were calculated from the leading terms of the second-order and first-order best fit curves, respectively. P was then calculated by dividing I by (NQ) for the op-EPSC elicited with 1-ms light stimulation. We validated MPFA at BLA synapses onto SST-INs following NASPM application to selectively attenuate AMPA receptor function (Figure S4).

To examine heterosynaptic interactions between BLA inputs and distal dendritic EPSCs, blue light stimulation of ChR2 preceded electrical stimulation of layer 1 across a range of ISIs [3,10,30,100,300 ms]. A baseline trace containing the optical EPSC alone was obtained by averaging 10 sweeps. At each ISI, the maximal difference in amplitude between the mixed EPSC and the baseline optical EPSC was obtained. These values were averaged across 3–4 replications and normalized to the isolated electrical EPSC in each cell. In similar experiments designed to examine interactions between BLA and MDT inputs, red light stimulation of Chrimson preceded blue light stimulation of ChR2. To mitigate concerns regarding opsin spectral overlap (i.e. blue light stimulation of Chrimson), saturating red light stimulation parameters were selected such that minimal EPSCs were detected following short latency blue light stimulation in slices expressing Chrimson but not ChR2 (Figure S7).

For studies examining inhibitory postsynaptic currents (IPSCs) evoked by ChR2 stimulation of SST-INs, pyramidal cells were held at -60 mV using the potassium-based internal solution. For studies examining spontaneous IPSCs (sIPSCs) and I/E ratios, a

cesium-based internal solution was used (in mM): 140 CsMeSO₃, 5 NaCl, 10 HEPES, 0.2 EGTA, 2 MgATP, 0.2 NaGTP, 5 QX-314. Cells were voltage-clamped at 0 mV near the reversal potential for monovalent cations. When multiple cells were collected from the same slice, the stimulation parameters from the first cell were used throughout. IPSC to EPSC (I/E) ratios were obtained by averaging the amplitude of 30 consecutive EPSCs and dividing by the average amplitude of 30 consecutive IPSCs at 0 mV. The coefficient of variation (CV) was taken as the standard deviation of responses divided by its mean. Jitter was defined as the standard deviation of the onset latency. asEPSCs, sEPSCs, and sIPSCs, were all identified using predefined templates in ClampFit software.

DART

We leveraged the second-generation DART2.0 system, which offers a wider dosing window than its predecessor (Shields et al., 2017). To select SST-INs as the target of DART manipulation, we injected 600 nL of 2e12 vg/mL AAV10-CAG-FLEX-HaloTag-DART2.0-2A-dTomato-WPRE (HT+) or AAV10-CAG-FLEX-ddHaloTagDART2.0-2A-dTomato-WPRE (HT-) into PFC of SST-Cre mice. Mice were given 3 to 4 weeks to allow for viral expression prior to preparation of acute brain slices. Prior characterization of YM90K-DART indicates that its pharmacophore is a specific antagonist for AMPA receptors, with no impact on the *N*-methyl-D-aspartate receptor nor significant off-target activity in a screen of 30 brain-enriched receptors (Shields et al., 2017).

RNA scope fluorescence-based *in situ* hybridization

Slices containing PFC were prepared and processed as described (Dogra et al., 2021). In brief, brains were dissected, flash-frozen on dry ice, and stored in cryo-embedding medium at -80 °C until thin sectioning (16 μm). The following steps were performed at room temperature unless otherwise noted. Slides were fixed in 4% paraformaldehyde for 20 minutes at 4 °C, immediately followed by dehydration with 50% ethanol (5 minutes), 70% ethanol (5 minutes), and twice with 100% ethanol (5 minutes). After dehydration, slides were dried for 5 minutes on absorbent paper. Sections were then incubated with Protease IV solution for 30 minutes, washed twice with PBS, and then incubated for 2 hours at 40 °C with probes for cellular subtype markers (*Sst* and *Parv*) and a probe we designed to recognize the gene sequence targeted for excision in *Grm5^{fl/fl}* mice (ACDBio, key resources table). Following additional washes and amplification steps, DAPI was applied for 30 seconds. Slides were imaged on a confocal microscope (Zeiss LSM 710). Images were collected with xyz acquisition mode such that the total thickness of sample ranged between 5–7 μm. Optical sections were projected onto a single image using Zen 2.6 software and fluorescence signals were quantified using Imaris analysis and ImageJ software. Cells with more than 2 puncta of *Grm5* transcript were considered positive.

Open field

Mouse movement was tracked by infrared beam breaks within an open field housed inside a sound-attenuating cabinet (ENV-510 and MED-OFA-022, MedAssociates) without any prior habituation to the chamber.

Elevated zero-maze

The elevated zero-maze was performed in a raised, annular maze with tinted plexiglass walls. The maze was split into four arm quadrants where two sections were open and the other two enclosed with walls. Mouse movement was tracked with ANYmaze software and percent time in each arm and distance traveled were analyzed.

Y maze

Spontaneous alternation was performed in a Y-shaped maze with clear, plexiglass walls. Mice were placed in one arm of the maze facing the center and could freely explore for 10 min. Animal tracking was performed using ANYmaze software with predetermined zones. A correct spontaneous alternation occurred when the mouse entered a different arm in each of three consecutive arm entries (e.g. ABC or BAC). Baseline sessions were conducted under low light conditions. Stress sessions were conducted in the same subjects at least one week later under ambient lighting.

Progressive ratio

Mice were trained to holepoke for access to a palatable liquid food (Ensure, 50% v/v 10 μL per delivery) on a progressive ratio schedule of reinforcement without food restriction as described (Gould et al., 2015; Joffe et al., 2017). Restraint stress was delivered after stable performance was acquired (<20% variation on 3 consecutive days without an upward or downward trend).

Fear conditioning

Mice underwent cued fear conditioning as described (Cummings and Clem, 2020; Maksymetz et al., 2019). Freezing behavior was assessed using VideoFreeze software (MedAssociates, St. Albans, VT) during a 2-minute baseline period and across a series of 5, co-terminating tone-shock pairings (30-s, 90 dB, 5000 Hz; 1-s, 0.7 mA). The data included in the manuscript arose from two cohorts of mice independently run by men (MEJ and JM). A third cohort was run by two women (DJL, assisted by IMG). In that cohort, female knockout mice displayed a trend towards decreased conditioned freezing, but male knockout mice displayed increased freezing relative to controls. No data from that cohort are included in this publication. Experimenter sex has been previously reported to affect stress-related behaviors (Sorge et al., 2014).

Operant discrimination

Operant experiments were performed in a standard Skinner box (Med Associates) equipped with 2 nose-poke ports (active and inactive, counterbalanced for side across animals), stimulus lights situated directly above each nose-poke, and a liquid delivery port equipped with an infrared beam for head-entry detection. A houselight and a speaker for white noise were located on the wall opposite of the liquid delivery port. The beginning of operant sessions was signaled by the onset of white noise (65dB) which remained on throughout the duration of each session. Mice were first trained to respond for sucrose during daily 1-hour sessions where responding in a nose-poke was reinforced on a fixed-ratio 1 schedule of reinforcement. The active nose-poke and a stimulus light located directly above the active nose-poke remained illuminated throughout the duration of the session. A response in the active nose-poke resulted in the delivery of sucrose in the liquid port (10% sucrose w/v, 10 μ L per delivery) while a response in the inactive nose-poke was recorded but had no programmed consequence. Animals advanced to the discrimination learning phase of the experiment following 2 consecutive days in which a minimum of 20 active nose-poke responses were recorded and a criterion of 70% responding on the active nose poke was achieved. Following acquisition of operant responding, animals were next trained to respond under the control of a discriminative stimulus (S^d). The apparatus and task parameters remained identical except for the following. Unlike during acquisition, the active nose-poke and associated stimulus light were not illuminated at the start of the session. Illumination of the nose-poke and light instead functioned as an S^d which indicated that a response would result in delivery of sucrose in the liquid port (reinforced responses are referred to as a 'correct response' throughout). The S^d was presented on a variable time 30 second schedule (20-40 second distribution, average of 30 seconds), and was terminated following a correct response or after a 30-second stimulus presentation period had elapsed. A response on the active nose-poke in the absence of the S^d (i.e., during the intertrial interval) did not result in sucrose delivery and instead triggered a 30-second timeout period signaled by illumination of a house light. The houselight was terminated at the end of the timeout period and the intertrial interval resumed until the onset of the next trial or until another timeout period was triggered. A discrimination index was calculated as the ratio of correct completions over both correct responses and timeouts triggered. A value of 0.5 indicates equal probability of making a response in the presence or absence of the S^d , while a value of 1 indicates that responding only occurs in the presence of the S^d .

Fiber photometry

Fiberoptic patch cables (400- μ m 0.48 NA, Thor Labs) were attached to each implant with a zirconia sleeve. Recordings were made with a LUX RZ5X processor (Tucker-Davis Technology) and specialized Synapse software. Two LEDs (405-nm and 465-nm) provided 20-50 μ W light to the brain and emitted light returned through a 500-540 nm filter to a Femtowatt Photoreceiver (Newport). Mice were habituated to tethering for 10 minutes one-day prior to recordings. On the day of testing, mice were connected to fiberoptic cables for 5 minutes in a novel cage prior to undergoing restraint stress in a custom device. Video recordings were made at 10 frames per second with a synchronized webcam (Logitech C920) and DeepLabCut software was used to analyze all behavioral recordings (Luchsinger et al., 2021; Mathis et al., 2018; Nath et al., 2019). Two points, the tip of the tail and a point on the fiberoptic cable about 3cm from the junction with the cannula were tracked over time based on previous methods used for manual scoring. We used a training set of >15 images per video to train DeepLabCut for at least 200,000 iterations. The derivative of the X and Y positions of the tail and the fiber were then calculated using R statistical software with the tidyverse package (R Development Core Team, 2018; Wickham et al., 2019). Movements were identified when frames with the velocity exceeded one standard deviation above baseline. Struggling episodes were defined when the tail and fiber underwent simultaneous movement at least 5 seconds past the onset of the previous episode. Signals were processed in MATLAB using customized procedures based off publicly available code (Akam and Walton, 2019). The calcium-dependent 465-nm signal and the isobestic 405-nm control signal were processed and analyzed separately without any corrections for presumed movement artifacts. Signals were down-sampled to \sim 100 Hz and processed with a median filter and a 10-Hz low-pass filter to remove artifacts and noise. Photobleaching was corrected with a 0.001 Hz high-pass filter and values were then normalized to a 0.001 Hz low-pass filtered signal and multiplied by 100. For each struggling episode, the area under the curve was obtained as the integral of the 5-second period following event onset and the maximal $\Delta F/F$ as the maximum amplitude during that same window. Both values were taken as the difference relative to the respective mean from 1-2 seconds preceding the event. For each subject, the AUC and $\Delta F/F$ values were binned across each third of the restraint stress session (i.e. [0:00-6:40]; [6:40-13:20]; [13:20-20:00]) and the median value for each bin was obtained.

QUANTIFICATION AND STATISTICAL ANALYSIS

The numbers of cells and mice are respectively denoted by "n" and "N". Data are presented in bar or symbol plots as mean \pm standard error or in box plots with median, interquartile range, and range. Averaging responses, calculating variances, and curve-fitting were performed in Microsoft Excel. Statistical analyses were performed in GraphPad Prism 9. Two-tailed Student's t-test and one- or two-way ANOVA were used as appropriate. Where significant (α : 0.05) interactions or main effects were detected, we used Sidak post-hoc comparisons to assess specific differences. Statistical findings are displayed in the figures or legends. Statistical outliers were removed using the ROUT test (Q=5%).